



## RESEARCH ARTICLE

10.1029/2021JG006332

### Key Points:

- In the high turbid nearshore, floc size varies with tides and seasons. In the low turbid offshore, floc size shows a seasonal signal
- Floc size increases with fresh transparent exopolymer particle (TEP), which is present in spring and summer. Mineral-associated TEP has little influence on floc size
- A model separates between fresh and mineral-associated TEP

### Correspondence to:

M. Fettweis,  
[michael.fettweis@naturalsciences.be](mailto:michael.fettweis@naturalsciences.be)

### Citation:

Fettweis, M., Schartau, M., Desmit, X., Lee, B. J., Terseleer, N., Van der Zande, D., et al. (2022). Organic matter composition of biomineral flocs and its influence on suspended particulate matter dynamics along a nearshore to offshore transect. *Journal of Geophysical Research: Biogeosciences*, 127, e2021JG006332. <https://doi.org/10.1029/2021JG006332>

Received 8 MAR 2021  
Accepted 14 DEC 2021

### Author Contributions:

**Conceptualization:** Michael Fettweis, Markus Schartau, Xavier Desmit, Nathan Terseleer

**Formal analysis:** Michael Fettweis, Xavier Desmit, Byung Joon Lee, Nathan Terseleer, Dimitry Van der Zande, Koen Parmentier

**Funding acquisition:** Michael Fettweis, Xavier Desmit

**Methodology:** Michael Fettweis, Xavier Desmit, Nathan Terseleer







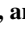

**Software:** Markus Schartau

**Visualization:** Michael Fettweis

**Writing – original draft:** Michael Fettweis, Dimitry Van der Zande

**Writing – review & editing:** Markus Schartau, Xavier Desmit, Byung Joon

# Organic Matter Composition of Biomineral Flocs and Its Influence on Suspended Particulate Matter Dynamics Along a Nearshore to Offshore Transect

Michael Fettweis<sup>1</sup> , Markus Schartau<sup>2</sup> , Xavier Desmit<sup>1</sup> , Byung Joon Lee<sup>3</sup> , Nathan Terseleer<sup>1</sup> , Dimitry Van der Zande<sup>1</sup> , Koen Parmentier<sup>1</sup> , and Rolf Riethmüller<sup>4</sup> 

<sup>1</sup>OD Natural Environment, Royal Belgian Institute of Natural Sciences, Brussels, Belgium, <sup>2</sup>GEOMAR Helmholtz Centre for Ocean Research Kiel, Kiel, Germany, <sup>3</sup>Department of Advanced Science and Technology Convergence, Kyungpook National University, Sangju, South Korea, <sup>4</sup>Institute of Coastal Ocean Dynamics, Helmholtz Centre Hereon, Geesthacht, Germany

**Abstract** The seasonal variation in concentration of transparent exopolymer particles (TEPs), particulate organic carbon (POC) and particulate organic nitrogen (PON) were investigated together with floc size and the concentration of suspended particulate matter (SPM) along the cross-shore gradient, from the high turbid nearshore toward the low-turbid offshore waters in the Southern Bight of the North Sea. Our data demonstrate that biophysical flocculation cannot be explained by these heterogeneous parameters, but requires a distinction between a more reactive labile (“fresh”) and a less reactive refractory (“mineral-associated”) fraction. Based on all data, we separated the labile and mineral-associated POC, PON, and TEP using a semi-empirical model approach. The model's estimates of fresh and mineral-associated organic matter (OM) show that great parts of the POC, PON, and TEP are associated with suspended minerals, which are present in the water column throughout the year, whereas the occurrence of fresh TEP, POC, and PON is restricted to spring and summer months. In spite of a constantly high abundance of total TEP throughout the entire year, it is its fresh fraction that promotes the formation of larger and faster sinking biomineral flocs, thereby contributing to reducing the SPM concentration in the water column over spring and summer. Our results show that the different components of the SPM, such as minerals, extracellular OM and living organisms, form an integrated dynamic system with direct interactions and feedback controls.

**Plain Language Summary** Particles suspended in coastal waters occur as loose aggregates of tiny mineral and organic particles, also known as flocs. Their mass concentration is higher in winter than in summer, but their sizes are smaller in winter. The seasonal cycle of phytoplankton activity drives this phenomenon. In spring, phytoplankton blooms and starts to produce fresh and sticky organic matter. This glue binds particles together after collisions and promotes increasingly larger and yet stable flocs. Analytical lab methods cannot distinguish between the freshly produced sticky and the older inactive organic material that is stored in the sediments and entrained into the water by erosion and resuspension. Therefore, previous studies were not able to detect the relation between the occurrence of the sticky material and the floc-sizes in coastal waters. However, our innovative model approach allows a separation into both fractions. We observe a clear increase in floc sizes during spring and summer when fresh sticky organic material is available. As larger particles sink faster, they are removed from the water column, which allows a higher light penetration. In this way, phytoplankton is exposed to changing conditions, an illustration of how direct interactions and feedback loops occur in an integrated dynamic system.

## 1. Introduction

The particulate organic matter (POM) is, together with particulate inorganic matter (PIM), the main component of the suspended particulate matter (SPM) in marine ecosystems. The flux and export of mineral and organic particles depends on flocculation processes, which influence the particles' composition and settling velocity. Flocculation combines organic and mineral particles into biomineral flocs (B. J. Lee et al., 2019; Shen et al., 2018; Skinnebach et al., 2020; Verney et al., 2009), which overcompensates the resulting decrease in overall density and therefore yields higher settling velocities compared to most of their constituents (e.g., Bach et al., 2019; Engel & Schartau, 1999; Fall et al., 2021; Manning & Bass, 2006; Manning et al., 2011; Neumann et al., 2019). In tidally dominated, mostly shallow environments, floc break-up dominates during periods of high currents and

© 2021. The Authors.

This is an open access article under the terms of the [Creative Commons Attribution License](https://creativecommons.org/licenses/by/4.0/), which permits use, distribution and reproduction in any medium, provided the original work is properly cited.

Lee, Nathan Terseleer, Dmitry Van der Zande

waves with strong shear. In contrast, the formation of larger flocs prevails during slack water periods (e.g., J. C. Winterwerp, 1998). The size of the flocs is theoretically determined by the smallest turbulent eddies (Braithwaite et al., 2012). But, floc size can exceed those in the presence of biogenic particles whose surfaces can become exceedingly sticky (Cross et al., 2013).

The interactions between hydrodynamic and atmospheric forcing, biological and chemical processes, terrestrial export and human activities affect concentration, composition, size, and density of biomineral flocs on various spatial and temporal scales (Capuzzo et al., 2015; Eisma & Kalf, 1979; Fettweis et al., 2006; Jago et al., 2007; Liénart et al., 2017). Characteristic for many shelf seas is the seasonality in SPM concentration. In the North Sea, the SPM concentration is higher in winter and lower in summer (Howarth et al., 1994). This seasonality appears to be caused mainly by biological cycles and only to a minor part by the higher storm frequencies in winter (Fettweis et al., 2014; Lai et al., 2018). Biological processes influence flocculation, seabed erodibility, and transport of the suspended particles, because of the emergence of polysaccharides such as exopolymeric substances (EPSs; e.g., Verdugo, 2012), including gel-like particles like transparent exopolymer particles (TEPs; e.g., Alldredge et al., 1993; Logan et al., 1995) and Coomassie stainable particles (e.g., Long & Azam, 1996). Dissolved EPS are the precursors of these particles and refer to any extracellular dissolved organic matter (OM) released from phytoplankton and bacteria, either actively by exudation or passively via viral lysis, sloppy feeding or through bacterial degradation (Engel & Passow, 2001; Engel et al., 2020; Passow, 2000). TEP are known to be a common component of the OM in marine environments, having specific characteristics such as adhesiveness, transparency, flexibility, and the ability to form biofilms (Mari & Robert, 2008; Passow, 2002; Zhou et al., 1998).

The interactions between TEP and SPM have mainly been studied in open ocean where mineral concentrations are low and the hydrodynamics is weaker than in coastal regions. Typically, under open ocean conditions TEP concentrations are correlated with the rise and decline of phytoplankton blooms (Fukao et al., 2010; Mari et al., 2017). In nearshore and estuarine environments, the hydrodynamical forces are strong and interdependencies between TEP and SPM become more complex. Measurements of TEP in combination with SPM concentration are scarce. So far published data reveal a seasonal variation, with high SPM concentration in winter, along with increased concentrations of OM, including TEP, displaying maxima within high turbid areas (Horemans et al., 2021; Malpezzi et al., 2013; Morelle et al., 2018). The SPM and TEP concentrations appear to be well correlated. During the spring and summer period this positive correlation persists, and reduced concentrations of SPM are accompanied with lowered TEP concentrations. Thus, the seasonal signal of observed TEP concentrations is unlike what is observed in the ocean. The observed seasonal development of TEP contradicts expectations and some specific dependencies between SPM and TEP have to be accounted for. In addition, there is no correlation between TEP and floc size in turbid coastal systems.

To resolve this apparent discrepancy, we here consider a separation between distinctive OM fractions of SPM (Blattmann et al., 2019; Schartau et al., 2019). The simplest distinction describes two forms of OM: (a) a freshly produced, free floating OM and (b) a mineral-associated, more refractory OM. As TEP is part of the OM, it is also subject to this partition. We hypothesize that the fresh part of TEP follows the seasonal development similar to open ocean conditions, thereby accumulating during spring and causing an increase in floc size, as observed in spring and summer. We hypothesize that the stickiness of the mineral-associated TEP is such that it contributes only marginally to flocculation. We hypothesize that TEP in offshore waters is dominated by fresh TEP (like in the ocean) while TEP in coastal waters is dominated by mineral-associated TEP. From these hypotheses, we expect that, in both offshore and coastal waters, the seasonal cycle of fresh TEP is paramount to understand the dynamics of SPM and water clarity.

The aim of our study is to test these hypotheses on the Belgian Continental Shelf (BCS) through data analysis (from in situ and remote sensing sources). This paper is structured in three parts. First, the fresh and mineral-associated POM concentrations in the particulate organic carbon (POC), particulate organic nitrogen (PON), and TEP fractions are differentiated through the use and refinement of the POM-SPM modeling approach of Schartau et al. (2019). Second, the seasonality of the size and density of biomineral flocs along the coastal-offshore gradient, as measured in situ, is related to fresh and mineral-associated POM. Third, the model is also applied to estimate fresh and mineral-associated POM from in situ optical backscatter sensor (OBS) and satellite SPM concentration measurements to discuss the temporal and geographical variability of SPM composition along the coastal-offshore gradient.

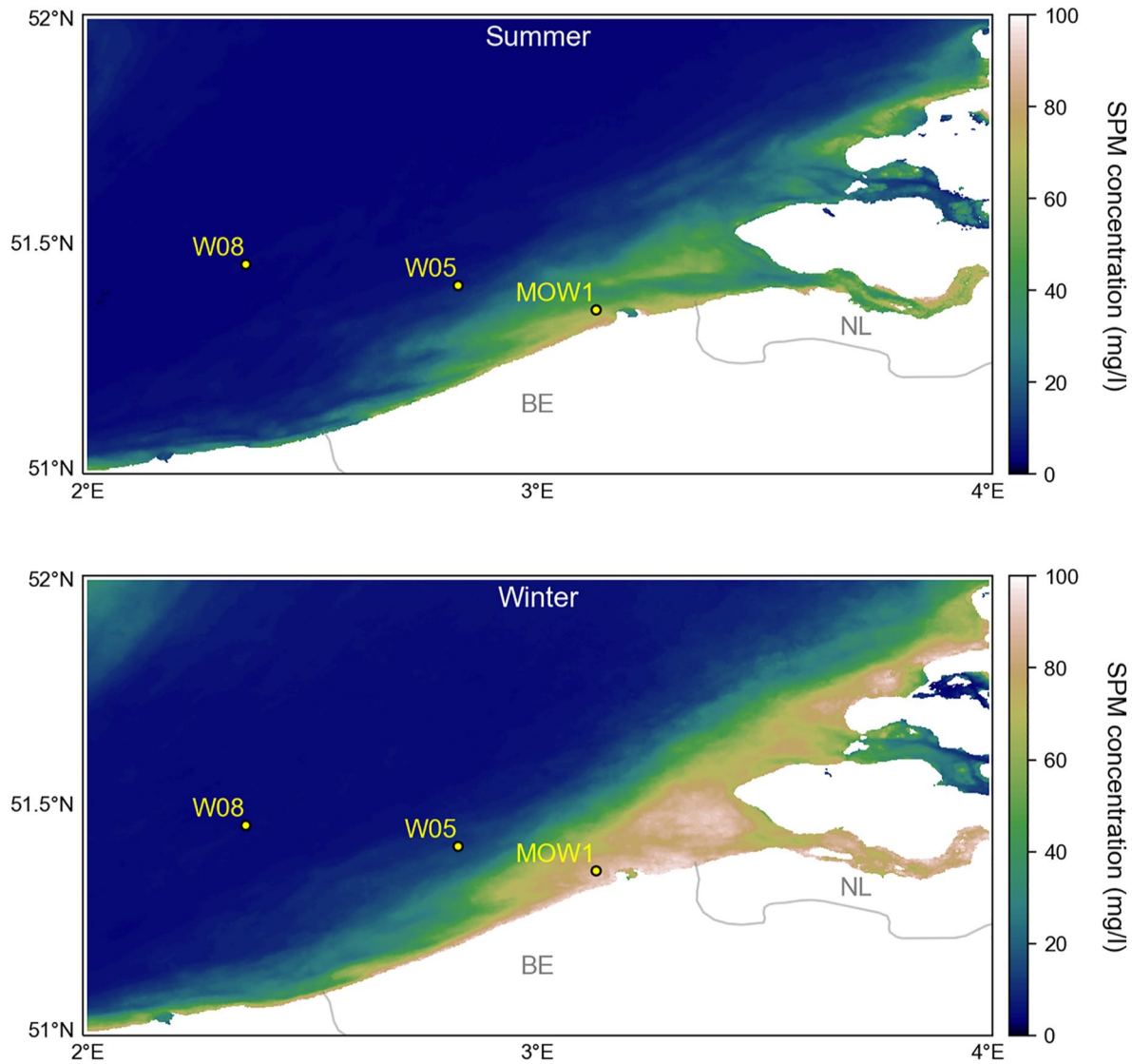


**Figure 1.** Map of sampling stations MOW1, W05, and W08 (BE: Belgium, NL: The Netherlands). The background displays the averaged near surface suspended particulate matter concentrations in the southern North Sea computed from satellite images taken by Sentinel-3/OLCI from April 2019 to September 2019 (above) and from November 2019 to March 2020 (below).

## 2. Methods

### 2.1. Measuring Strategy

#### 2.1.1. Water and Seabed Samples

The water sample data were taken on the BCS between October 2004 and August 2020. The data set consists of hourly (or 1.5 hourly) water samples and particle size distributions collected during 125 tidal cycles (sometimes half tidal cycles) in 12 stations. The three main stations (MOW1, W05, and W08, Figure 1) are located along a cross-shore section that ranges from the nearshore coastal turbidity maximum (MOW1) to the offshore under complete Channel water influence (W08). W05 is located in between at the outer margin of the coastal turbidity maximum. At W05 and MOW1 Channel waters still dominate, although fresh waters from the Rhine-Meuse and the Scheldt consist of about 6% at MOW1 (Lacroix et al., 2004). The present-day SPM in the coastal turbidity maximum originates mainly from the erosion and resuspension of the existing mud deposits situated in the Belgian nearshore (Adriaens et al., 2018).

From 2004 until 2011 the measured parameters were SPM, POC, PON concentrations and salinity. Concentration measurements of chlorophyll-a (Chl-a) and pheophytin-a (Pheo-a) were added from 2012 onward. All the samples collected until March 2018 were taken at about 3 m above the bed. From March 2018 onward near surface samples were also collected and the turbidity of the samples was measured with a Hach TL2360 LED Turbidimeter. From December 2018 onward, observations also covered TEP, dissolved organic carbon (DOC) and inorganic nutrient concentrations, the number of stations was reduced to 3 (MOW1, W05, and W08) while the frequency increased to monthly samplings. The measured dissolved components were only sampled at the surface, as the water column is well mixed throughout the entire year. Six Van Veen grab samples have been taken in each of the main stations in 2019 for the analysis of POC and PON content in the <63  $\mu\text{m}$  fraction.

The amount of SPM-POC, SPM-PON, and SPM-TEP data pairs is equal to 1,900, 1,719, and 598, respectively. All the TEP data and about 80% of the POC and PON data are from the three main stations.

### 2.1.2. Sensor Measurements

A LISST 100X was attached to the rosette to measure volume concentrations in 32 logarithmically spaced size groups over the range of 2.5–500  $\mu\text{m}$  using laser diffraction (Agrawal & Pottsmith, 2000). Long-term measurements with a LISST 100X (type C) and an OBS are available at the station MOW1 from tripod deployments over the period 2005–2019. In the beginning, the tripod was moored for 3–6 weeks and then recovered. From December 2009 an advanced tripod system allowed continuous time series. The LISST 100X was mounted at 2 m above bed (mab) and the OBS at 0.2 and 2 mab. In total about 1,716 days of “good” LISST data have been collected and about the double of “good” OBS data. “Good” LISST data are defined by a smooth (i.e., no sudden decrease) optical transmission within a range between 0.15 and 0.98, a smooth floc size distribution (FSD) and no biofouling. The latter two disturbances have regularly been observed in the long-term data series. Disturbed FSDs occur when the laser beam is misaligned. Biofouling occurs mainly in spring and summer and is identified by a gradual decrease in transmission or optical backscatter and increase in SPM volume concentration.

OBS data have been discarded when the sensor output changed over time unrelated to changes in inherent particle properties or SPM concentration (Fettweis et al., 2019). The OBS output is sensitive to cross sectional area and composition of the particles in suspension (Downing, 2006; Fettweis et al., 2019). At the measuring location the SPM consisted of flocs and occasionally sand in suspension. The OBS measurements of flocs are linearly related to SPM concentration by mass and thus well suited for flocs (Downing, 2006). In case of sand in suspension, which might occur during maximum current velocities, the OBS output will underestimate the SPM concentration. The OBS output were first calibrated against a laboratory standard (AMCO clear) to convert the sensor output to a backscatter turbidity unit, before being calibrated in situ with SPM concentration derived from water samples to obtain a mass concentration. The OBS mounted at the tripod were calibrated about every 2 months, so that seasonal variations in the particle composition have been considered.

### 2.1.3. Remote Sensing Measurements

Surface SPM and Chl concentration have been derived from the Ocean and Land Color Instrument (OLCI). OLCI is a multispectral radiometer carried on board Sentinel-3A (launched in 2016) and B (launched in 2018) with 21 bands on the 400–1,200 nm spectral range and a spatial resolution of 300 m. The two satellites provide a daily revisit time over the southern North Sea. Sentinel-3/OLCI baseline water products (L2-WFR) were retrieved from the Copernicus Online Data Access service hosted by EUMETSAT (coda.eumetsat.int). The baseline products were processed with IPF-OL-2 version 06.13 (EUMETSAT, 2019) with standard masking applied, that is, excluding INVALID, LAND, CLOUD, CLOUD\_AMBIGUOUS, and CLOUD\_MARGIN pixels. Additionally, a custom quality control was applied to remove outlier pixels with a spectrally flat signal. The SPM product was generated by an artificial neural network as a multiple non-linear regression technique to deal with the optically complex waters in the study area. The artificial neural network, originally developed by Doerffer and Schiller (2007), was updated to become the Case 2 Regional (C2RCC) processor suitable for Sentinel-3 (EUMETSAT, 2019).

The derivation of reliable satellite estimates of Chl-a in optically complex coastal waters had been elaborated with the approach of Lavigne et al. (2021), accounting for the fact that many existing algorithms perform differently under different optical conditions. Lavigne et al. (2021) clearly defined the limits of applicability of three popular and complementary algorithms: (a) the OC4 blue-green band ratio algorithm, which was designed for open ocean waters; (b) the OC5 algorithm, which is based on look-up tables and corrects OC4 overestimation in

moderately turbid waters; and (c) a near infrared-red (NIR-red) band ratio algorithm designed for high turbid waters. We followed their approach and allowed for automatic pixel-based switching between the most appropriate algorithms for a certain water type. For the measuring stations these are depending on the season, OC4 and OC5 for W08, OC5 and NIR-red for W05, and NIR-red for MOW1.

## 2.2. Sample and Data Analysis

### 2.2.1. Water Samples

At every sampling occasion, three subsamples for SPM concentration were taken and filtered on board using pre-combusted (405°C, 24 hr), rinsed, dried for 24 hr at 105°C and pre-weighted 47 mm GF/C filters. After sampling the filters were rinsed with ultrapure water (resistivity 18.2 MΩcm normalized at 25°C) and immediately stored at −20°C, before being dried during 24 hr at 50°C and weighted to obtain the concentration. The uncertainty (expressed as the RMSE of the triplicates divided by the mean value) decreases with increasing concentration from 8.5% (SPM concentration <5 mg/l) to 6.7% (<10 mg/l), 3.5% (10–50 mg/l), and 2.1% (>100 mg/l) and represent the random error related to the lack of precision during filtrations. Especially in clearer water, systematic errors due to the offset by salt or other errors become much larger than the random errors (Fettweis et al., 2019; Neukermans et al., 2012). These are not included, and have been estimated based on Stavn et al. (2009) and Röttgers et al. (2014) as 1 mg/l. The samples for POC and PON were filtered on board using 25 mm GF/C filters (pretreated as above for SPM), stored immediately at −20°C, before being analyzed using a Thermo Finnigan Flash EA1112 elemental analyzer (for details see Ehrhardt & Koeve, 1999). The analytical uncertainty for POC and PON are 12% and 18%. The method for TEP analysis follows the one described in Nosaka et al. (2017). This method is, as many other semi-quantitative methods, based on Alldredge et al. (1993) and Passow and Alldredge (1995). Three subsamples for TEP concentration were filtered using 25 mm 0.4 μm polycarbonate filters with low under-pressure (<200 hPa). The filters were colored immediately after filtration with Alcian blue and stored at −20°C. The stained particles are related to a weight equivalent for the anion density of TEP and standardized using xanthan gum (Passow, 2002; Passow & Alldredge, 1995). The units for TEP are expressed as mg xanthan gum equivalents per liter (mg XG eq./l) and the uncertainty is assumed to be equal to the one of POC. The sample for pigment concentration was filtered on 47 mm GF/C filters, stored in liquid nitrogen and determined in the lab using ultra high-performance liquid chromatography with fluorometric detection. The filtrates were collected in sample tubes for DOC and inorganic nutrients and analyzed using standard spectrophotometric methods with a Skalar autoanalyzer, for details see van der Zee and Chou (2005).

### 2.2.2. Sediment Samples

The POC and PON content of the bed surface samples was determined for the fraction <63 μm using the same method as described above.

### 2.2.3. Floc Size Distribution and Effective Floc Density

The volume concentration of each size class is used to build the FSD, and thus the median floc size (D50) and total SPM volume concentration are computed from the FSDs. The uncertainties and limitations of the LISST 100X detectors are related to the shape, size and inherent optical properties of the particles occurring in nature, and to the measuring principle (Andrews et al., 2010; Davies et al., 2012; Mikkelsen et al., 2006; Schwarz et al., 2017) and will influence the FSD. The sensor emits a laser beam and detects the intensities of the light scattered by particles on 32 concentric ring detectors. These intensities are then inverted to estimate particle size distributions assuming spherical shapes (Agrawal & Pottsmith, 2000). However, natural particles such as flocs, have irregular shapes and generally follow Junge or multimodal log-normal distributions (e.g., Buonassissi & Dierssen, 2010; Liley, 1992). This introduces intrinsically a size distribution that renders the resulting FSD approximative (Davies et al., 2012; Fugate & Friedrichs, 2002; Mikkelsen et al., 2007; S. J. Smith & Friedrichs, 2011).

The median particle size of the FSD is an approximate value as particles outside the range of the instrument are pooled in the smallest and/or largest size classes (“rising tails”) and because the instrument underestimates the size of mono-sized particles (Andrews et al., 2010; Gartner et al., 2001; Graham et al., 2012) and thus also the volume concentration. These errors are of systematic nature, and reflect the lack of accuracy of the instruments. A rising tail in the lowest size classes of the LISST was frequently observed in the data from the turbid nearshore station MOW1 and is interpreted as an indication of the presence of very fine particles and thus a break-up of



the aggregates. The importance of these spurious results depends on the number of small and large particles in the distribution. Macrofloc sizes recorded by a video system at a turbid estuarine site with similar tidal dynamics as at MOW1 were generally smaller than 580 mm (J. Winterwerp et al., 2006), which indicates that most of the larger flocs are most probably not exceeding the size limit of the LISST in the turbid nearshore. In case of a too low turbidity (transmission >90%) the data becomes less accurate, this occurred regularly at the two offshore stations W05 and W08. Despite the uncertainties and limitations of the LISST-100X, which are related to the characteristics of the particles occurring in nature and to the measuring principle itself, it is well suited to collect long-time series of FSD autonomously.

The effective floc density ( $\rho_{\text{eff}}$ ) is the ratio of floc mass ( $M_f$ ) over floc volume ( $V_f$ ) minus the water density ( $\rho_w$ ). The floc mass,  $M_f$ , can be calculated as:

$$M_f = M_p + M_w = M_p + \rho_w(V_f - V_p) = M_p + \rho_w(V_f - M_p/\rho_p) \quad (1)$$

where  $\rho_p$  is the primary particle density,  $M_w$  is the mass of water, and  $M_p$  the mass of primary particles in the flocs. The latter can be obtained from the SPM filtrations, the water density was fixed at 1,025 kg/m<sup>3</sup>, the primary particle density was estimated based on the PIM and POM fraction in the SPM (Fall et al., 2021). The POM content was estimated by multiplying the POC content by a factor 4. The PIM and POM density was set to 2,500 and 1,100 kg/m<sup>3</sup>, respectively (Fettweis, 2008) and the floc volume is the volume concentration measured by the LISST. The uncertainty of the effective floc density has been estimated as 10% (Fettweis, 2008). The origin of the error is related to the determination of  $M_p$ ,  $V_p$  and  $\rho_p$ , but is probably higher. The variability in the densities of the heterogeneous primary particles, the statistical nature of primary particle distributions, and the fact that probably not all the OM is in the floc, make the exact determination of effective density difficult.

#### 2.2.4. Long-Term Measurements of the FSD and SPM Concentration

The structure of the long-term FSD time series at MOW1 has been investigated using the entropy analysis (e.g., Mikkelsen et al., 2007). Applied to FSDs, entropy analysis allows grouping the size spectra without assumptions about the shape of the spectra. It is therefore suited for analyzing unimodal as well as multimodal distributions. First, the 60 min averaged FSD time series were normalized by dividing each of the 32 size classes by the total volume concentration of the FSD and then pl64 low-pass filter (Beardsley et al., 1985) removed the tidal signal. Next, a climatological FSD over the period 2006–2019 was generated by averaging the data of each time stamp related to the start of the respective year. Finally, a climatological entropy classification was carried out using the FORTRAN routine of Johnston and Semple (1983). In accordance with Fettweis et al. (2014) four entropy groups have been chosen for the classification. The pl64 low-pass filter was also applied to the long-term SPM concentration time series before a climatological SPM concentration was calculated over the period 2005–2016 similar to the climatological FSD time series.

### 2.3. Model Based Differentiation of OM Between Fresh and Mineral-Associated Fractions

The inorganic and organic components of the SPM have different origins. The mineral particles may have a lithogenic or biogenic origin. The lithogenic PIM typically incorporates clays, quartz, and other minerals, while biogenic PIM consists of minerals such as carbonates and amorphous silicates. In the further considerations, we will only consider PIM as a whole. The POM is a mixture of compounds derived from marine photosynthesis or terrestrial sources. It is a combination of diverse detrital organic substances as well as of living organisms such as bacteria, phyto- and zooplankton. The mineral-associated POM appears to be more refractory than freshly produced POM, both having different susceptibilities toward microbial degradation (Arndt et al., 2013). We will use the adjectives “mineral-associated” (POM<sub>m</sub>) for the more refractory fraction and “fresh” (POM<sub>f</sub>) for the labile and semi-labile fraction. The POM<sub>m</sub> is incorporated in the mineral fraction where it is particularly bound with clay minerals (Blattmann et al., 2019; Mayer, 1994).

#### 2.3.1. Model Assumptions

For coastal and estuarine environments, estimates of the mineral-associated POM<sub>m</sub> and fresh POM<sub>f</sub> can be derived from a data-model synthesis (Schartau et al., 2019), provided that either POM or its subcomponents like POC, PON, or TEP have been measured jointly with SPM concentrations. Schartau et al. (2019) proposed a semi-empirical model of the POM:SPM ratio (measured as Loss on Ignition, LoI) as a function of SPM concentration.

After model calibration with LoI data, they documented the applicability and advancements of differentiating between  $POM_f$  and  $POM_m$ . The conceptual basis of the POM-SPM model is that the POM concentration can be written as the sum of the  $POM_f$  and  $POM_m$  concentrations. The  $POM_m$  is assumed to be linearly correlated with the PIM concentration by a constant proportionality factor  $m_{POM}$ :

$$POM = POM_f + POM_m = POM_f + m_{POM}PIM = POM_f + \frac{m_{POM}}{m_{POM} + 1}SPM \quad (2)$$

An additional assumption is that the seasonal build-up of  $POM_f$  can be described as a saturation function of the SPM concentration, assuming that primary production eventually becomes nutrient limited, although it may also depend on temperature and light availability. Thus, for high SPM concentrations, when  $POM_f$  has reached its maximum concentration (capacity of  $POM_f$  build-up) the  $POM_m$  fraction dominates the POM pool ( $POM:SPM \approx POM_m:SPM = m_{POM}/m_{POM} + 1$ ).

In the presence of mineral associated  $POM_m$  ( $m_{POM} > 0$ ), the fresh  $POM_f$  can be described as

$$POM_f = \frac{K_{POM}}{\frac{K_{POM}}{SPM} + 1} \frac{1}{m_{POM} + 1} \quad (3)$$

with the parameter  $K_{POM}$  (in the same units as SPM concentration) being the second parameter of the POM-SPM model. For  $m_{POM} = 0$  we note that Equation 3 reduces to the initial (baseline) formulation,  $POM_f = K_{POM} \times SPM / (K_{POM} + SPM)$ , introduced in Schartau et al. (2019; Equation 8 therein). The saturation concentration of  $POM_f$  is reached at high SPM concentrations ( $\approx K_{POM}/(1 + m_{POM})$  for  $SPM \gg K_{POM}$ ), which means that the  $POM_f$  fraction of the SPM ( $POM_f:SPM$ ) converges toward zero in high turbid areas.

Optimized values of  $K_{POM}$  were shown to vary seasonally (Schartau et al., 2019), depending on the amount of nutrients being readily transformed to  $POM_f$  and not yet being remineralized. In contrast, values estimated for  $m_{POM}$  turned out to be fairly constant and independent of seasonal conditions. Instead of using LoI data for POM content, we here considered three different types of OM data, namely the concentrations of POC, PON, and TEP. Therefore, the POM-SPM model had to be refined, introducing two parameters ( $f_1$  and  $f_2$ ) for every observational type  $X_i$  (POC, PON, and TEP):

$$X_i = X_{i,m} + X_{i,f} = f_{1,X_i}POM_f + f_{2,X_i}POM_m \quad (4)$$

These additional parameters,  $f_{1,X_i}$  and  $f_{2,X_i}$ , represent relative proportions of  $X_i$  to POM, for example,  $f_{1,PON}$  expresses the ratio of fresh PON to fresh POM and  $f_{2,PON}$  is the mineral associated  $PON_m$  mass fraction of  $POM_m$ . The parameters  $f_{1,X_i}$  and  $f_{2,X_i}$  for POC and PON are given in units of molecular weight ( $g\ g^{-1}$ ), but for TEP the conversions are given in units of ( $g\ XG\ eq.$ )/(g POM). In this manner, consistent and meaningful estimates of  $f_{1,X_i}$  and  $f_{2,X_i}$  could be derived. We stress that values estimated for  $K_{POM}$  and  $m_{POM}$  determine estimates of POM only, and these estimates should be independent of the observational type, no matter whether POC, PON, or TEP concentrations are considered. This implies that variations in  $K_{POM}$  estimates, for example, temporal trends, should become similarly resolved by using either of the available observational types, which is a rigorous and strict test of the credibility of the optimal parameter estimates.

### 2.3.2. Parameter Optimization

The semi-empirical model is fitted to the observations and its parameters are determined by statistical optimization. The mineral-associated  $POM_m$  of the SPM is entirely determined by the value assigned to the parameter  $m_{POM}$  (Equations 2 and 4). The parameters  $m_{POM}$  and  $f_2$  are collinear and therefore they cannot be estimated independently. For maintaining consistency between the previous parameter estimates of  $m_{POM}$ , and the added parameters of  $f_2$  ( $f_{2,POC}$ ,  $f_{2,PON}$ , and  $f_{2,TEP}$ ) we used the optimized value ( $m_{POM} = 0.13$ ) of Schartau et al. (2019). This estimate was obtained by using data of all seasons within the German Bight and German part of the Wadden Sea in the south-eastern region of the North Sea. The uncertainty of this estimate for  $m_{POM}$  is small (<3%) and the seasonal variations between estimates turned out to be small as well (0.12–0.14). With a fixed value assigned to  $m_{POM}$ , we only require values of three parameters to be optimized. The values of  $f_1$ ,  $f_2$ , and  $K_{POM}$  were estimated by minimizing the negative logarithm of a likelihood and a prior (cost function) that was used as a metric for assessing the deviation between observational data and the model counterparts. In general, for the likelihood (description of the data, given the model) and prior (deviation between estimated and some prescribed

characteristic parameter value) we assumed respective probability densities to be normal, represented as Gaussian functions of the data-model residuals and of the deviation of parameter estimates from a prior value assigned to  $K_{\text{POM}}$ . Reasons for why we had to account for prior information will be explained in the following paragraph. We explicitly accounted for uncertainties in the observations and in the prior value of  $K_{\text{POM}}$ . Optimal combinations of parameter values were determined for seasonally sorted data sets of POC, PON, and TEP. The observational data reveal pronounced variability at low SPM concentrations, which becomes much reduced at high SPM concentrations. At high SPM concentrations ( $>100$  mg/l), uncertainties in measurements were much lower than the variations due to spatio-temporal variability. Like in the approach of Schartau et al. (2019), we added the variance of the observed POC:SPM, PON:SPM, and TEP:SPM to the measurement uncertainties for SPM concentrations  $>100$  mg/l, otherwise individual data points at such high SPM concentrations can introduce severe biases in the estimates of the parameters  $f_1$  and  $K_{\text{POM}}$ . For all data points we calculated variances for POC:SPM, PON:SPM, and TEP:SPM, following the law of error propagation, based on individual measurement errors of SPM, POC, and PON concentrations. Errors for TEP were assumed to be 15% of the measured concentrations, which was approximately the highest relative error found for the POC concentration measurements.

The cost functions' minima yield the best model representations of the POC:SPM, PON:SPM, and TEP:SPM data. Respective minima (best parameter values) were identified by exploring the parameter space including combinations of the three parameters of interest,  $f_1$ ,  $f_2$ , and  $K_{\text{POM}}$ . Intervals and resolution differed between the observational types for  $f_1$  and  $f_2$ . For POC and TEP we chose  $f_1$  and  $f_2 \in [0.01, 1]$  with a resolution of  $\Delta = 0.01$  (with 100 elements respectively). For PON we had to increase the variational range and resolution for  $f_1 \in [10^{-3}, 1]$  (resolution  $\Delta = 10^{-3}$ ) as well as for  $f_2 \in [5 \times 10^{-4}, 1]$  ( $\Delta = 10^{-4}$ ). Possible values of  $K_{\text{POM}}$  span two orders of magnitude and we therefore assigned a constant resolution on logarithmic scale ( $\Delta \log = 5 \times 10^{-3}$ ) within the interval  $\log_{10}(K_{\text{POM}}) \in [\log_{10}(0.1), \log_{10}(10)]$ , which approximates a precision of 1%. The parameter screening is fast enough for deriving confidence intervals of respective parameter estimates via subsampling. A range of best parameter estimates was confined from 100 individual optimizations, based on random data subsamples that each included 30% of respective total data points. Doing so we learned that estimates of  $f_1$  can become poorly constrained (mainly when using autumn data) for some subsamples that yield estimates of  $K_{\text{POM}} < 0.5$  mg/l. By introducing an additional term as a prior to the likelihood-based cost function, the optimization problem became well-posed for all subsample cases and we could obtain robust parameter estimates. For the prior we imposed a  $K_{\text{POM}}$  value of 2.0 mg/l, with a 100% uncertainty ( $=2.0$  mg/l) for all seasons apart from autumn, for which we had to prescribe a 25% uncertainty ( $=0.5$  mg/l) for the prior. Based on the 100 individual optimizations, each with a different set of subsampled data, we determined statistical properties of the estimates, including lower and upper limits of 95% confidence intervals respectively. Instead of the arithmetic mean, the median of the parameter estimates turned out to be a better representation of the overall model fit to the data. This is because curved collinearities appeared in few cases and respective mean values did not coincide with the curved (banana-shaped) spread of optimal parameter values. In all other cases the median was similar to the mean of the estimates.

For model descriptions of POC:SPM and PON:SPM we considered seasonal variations and distinguished between in parameter estimates accordingly, combining data from 3 months: winter (December, January, and February), spring (March, April, and May), summer (June, July, and August), and autumn (September, October, and November). Monthly parameter estimates were elaborated for model fits to TEP:SPM data. Instead of using data from a single month, we included data from the two adjacent months. For example, optimal parameter values for January were constrained with data from December, January, and February. Likewise, in June the parameter estimates were determined with data from May, June, and July. We recommend such a procedure, because it facilitates the identification of gradual temporal changes in parameter estimates, similar to the low-pass filtering of a moving average.

### 3. Results

#### 3.1. Temporal and Spatial Variabilities

The seasonal variability of the main biogeochemical properties of the water at the three major sampling sites (MOW1, W05, and W08) along the coastal-offshore gradient together with some physical data are shown in Figure 2. The tidal amplitude (Figure 2a) has been calculated for Zeebrugge (close to MOW1) from harmonic analysis. The significant wave height is from a wave buoy near MOW1 (Figure 2b). It has been downloaded from the Measurement Network Flemish Banks (<https://meetnetvlaamsebanken.be>). The daily solar radiation at Zeebrugge



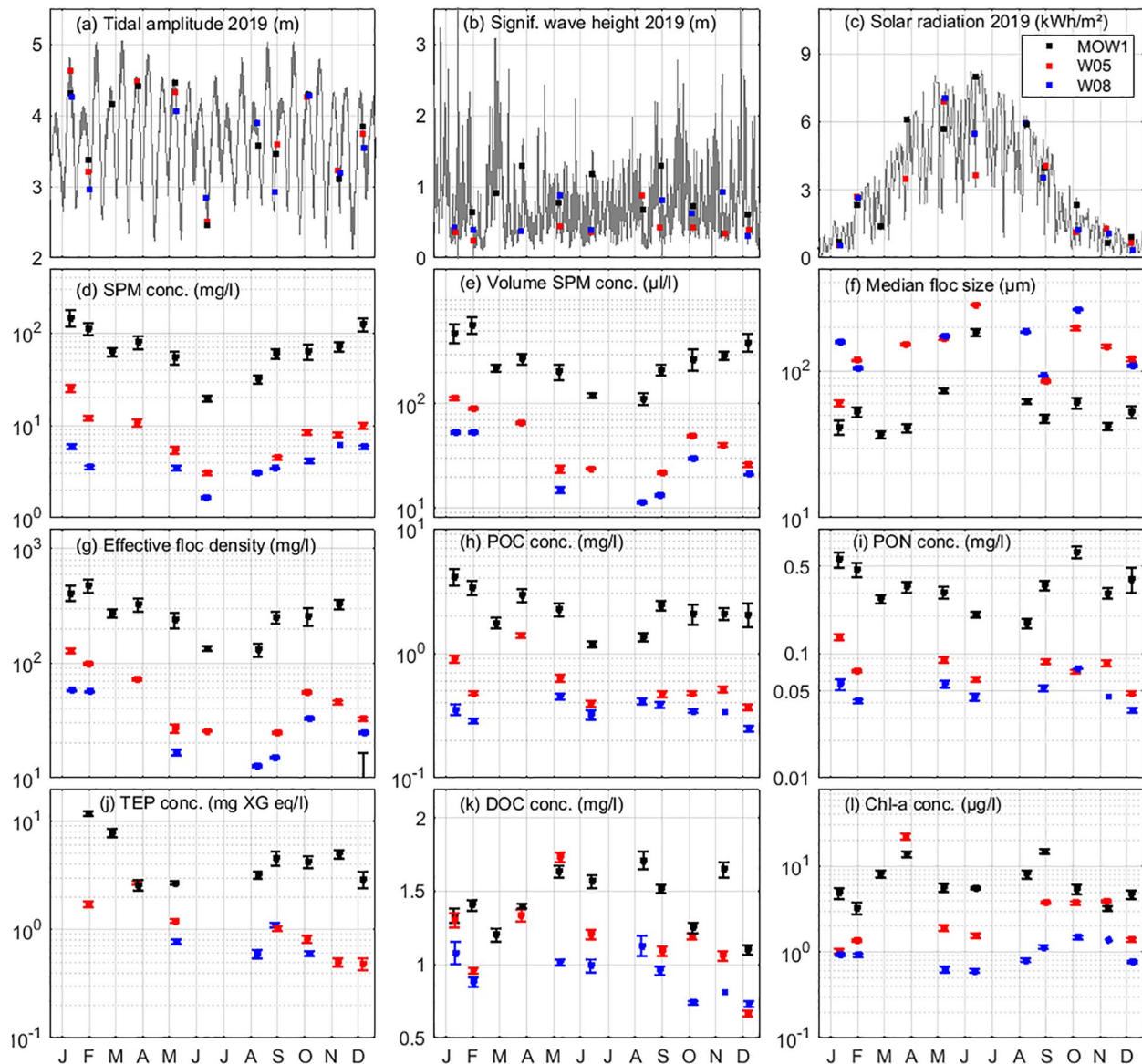


**Figure 2.** Physical (a) harmonic tidal amplitude, (b) significant wave height, (c) solar radiation), (d–i) particulate matter and (j–l) dissolved matter parameters from 2019 (transparent exopolymer particle is from 2019 until August 2020) versus time (see Section 2.1.1). For the particulate and dissolved parameters the geometric means over the tidal sampling period are shown with their standard errors of the mean at three sampling stations (MOW1: black, W05: red, and W08: blue).

(Figure 2c) has been obtained from the Royal Meteorological Institute (<https://www.meteo.be>). In situ data of dissolved and particulate matter have been averaged over the sampling period (usually 12 hr) and over the vertical. The data averaged over four seasons for all available parameters (2004–2020) are given in the Tables A1–A3 in Appendix A. For completeness, these tables also comprise parameters that are not further discussed in this study.

Variations in parameters occur at tidal, lunar and seasonal scales. Winter (December–February) is the period with low solar radiation, high nutrient concentration and low primary production. In spring (March–May) increasing solar radiation and temperature initiate phytoplankton blooms under nutrient replete conditions. Summer (June–August) has the highest solar radiations (Figure 2c) and nutrients are largely consumed. In late summer–early autumn, a second phytoplankton bloom shows up, but from autumn (September–November) on, phytoplankton activity ceases with the decreasing solar radiation and nutrients pile up again.

It is interesting to note that for the majority of parameters the more offshore stations W05 (red) and W08 (blue) displayed the same overall course as in MOW1 (black) but with lower values and a lower seasonal variability.

Exceptions are median floc size and salinity. Observed variability during a tidal cycle is also less pronounced in the offshore stations. The water column was well mixed in all stations, the variations in salinity between them are, in accordance with Lacroix et al. (2004), caused to a large part by different freshwater contributions from the Rhine-Meuse and the Scheldt rivers. Temperature varied during 2019 sampling between 6.0°C at MOW1 in January (6.3°C at W05 and 8.7°C at W08) and 19.9°C in June (19.5°C at W05 and 18.2°C at W08).

At each station, the highest SPM concentrations occurred in winter and the lowest in summer (Figures 1 and 2d). The volume SPM concentration has a nearly 75% more pronounced seasonality than the mass SPM concentration (Figures 2d and 2e and Tables A1–A3). The lower spring-summer volume SPM concentrations correspond to larger floc sizes (Figure 2f) and also to lower effective floc densities (Figure 2g). Median floc size increased toward offshore by about 2. POC and PON concentrations (Figures 2h and 2i) are correlated with SPM concentrations, although higher POC:SPM and PON:SPM ratios occurred during the spring phytoplankton bloom (see Tables A1–A3 in Appendix A). The yearly mean value of the POC/PON ratio is 6.61 molC molN<sup>-1</sup>, practically equal with the Redfield ratio (6.62 molN molC<sup>-1</sup>). Lower values occur in spring (6.37) and summer (6.06) and higher ones in winter (7.01) and autumn (6.75). According to Frigstad et al. (2011), this seasonal variation reflects variations in the water mass characteristics, nutrient concentrations, biomass and OM composition.

TEP concentration (Figure 2j) at MOW1 varied between 0.31 and 17.2 mg XG eq./l in winter, 0.62 and 17.57 mg XG eq./l in spring and 1.53 and 6.97 mg XG eq./l in summer. At W05 these values were between 0.11 and 3.31 mg XG eq./l (winter), 0.76 and 4.13 mg XG eq./l (spring) and 0.61 and 1.74 mg XG eq./l (summer); and at W08 between 0.10 and 0.59 mg XG eq./l (winter), 0.52 and 1.09 mg XG eq./l (spring) and 0.28–1.60 mg XG eq./l (summer). The seasonal variation in TEP concentration was similar to POC, PON, and SPM concentration and all were somewhat opposite to the DOC concentration (Figure 2k). Although patchy, DOC concentration had generally higher values in summer than in winter, which is explained by the production of DOC by phytoplankton in spring and summer and the subsequent slow degradation (Van Engeland et al., 2010).

Chl-a concentration (Figure 2l) was highest during the spring phytoplankton bloom. Except for the spring plankton bloom, the Chl-a concentration at MOW1 was higher than in the offshore stations. This is probably due to the higher availability of nutrients, in spite of the lower water clarity. The winter Chl-a concentrations reached values of a few µg/l in winter, and were thus of the same order of magnitude or even higher than the offshore concentrations in spring and summer. Pheophytin is one of the breakdown products of chlorophyll and is thus an index of decomposable OM Fuchs et al. (2002). The Pheo-a concentration had an opposite, although weaker, seasonal pattern than the Chl-a concentration. Inorganic nutrient concentrations (for example total dissolved nitrogen, total dissolved phosphate and silicates, see Tables A1–A3 in Appendix A) showed the typical pattern of the North Sea with relatively high concentrations in winter and low concentrations in summer due to nutrient utilization by phytoplankton (Lancelot et al., 2005).

### 3.2. Floc Size

Important to our demonstration, the seasonal (and tidal) variability of the FSD can be related to the seasonal growth of phytoplankton (and the current velocity during tidal cycles). Some hourly near-bed FSDs by volume measured during a tidal cycle are shown in Figure 3 for the three main stations for a winter, summer and autumn month. The FSDs measured by the LISST 100X during profiling cover the water column between about 2–3 m above bed and the surface. These data reveal that floc sizes near the surface are only slightly lower than those near the bed and that trends inferred from near-bed data can thus be considered equivalent to trends observed in surface waters. Common to all, the tidal changes in volume concentration are a result of deposition, resuspension/erosion and advection. The FSDs at MOW1 were more variable during a tide than at W05 and W08, meaning that break-up and aggregation are dominating the FSD. At W05 and W08, the particles' sizes were less variable during a tidal cycle. This points to stronger aggregates and particles of biological origin that are not subject to turbulence-driven flocculation processes. In spring and, to some extent, in autumn, the FSD at MOW1 became bimodal, with a main peak around 60 µm and a second one around 300 µm. The latter is an indication of the occurrence of large biomineral flocs (Shen et al., 2018). The FSDs at W05 and W08 were unimodal in spring with a peak at 300 µm. In early autumn (September) and in winter they became bimodal, with a secondary peak at around 70 µm (winter) or 100 µm (early autumn). The winter FSD at W05 was more variable as it is located at the edge of the turbidity maximum zone. When the turbidity is higher, then the FSD resembles that of MOW1, in the opposite case it is similar to the offshore station W08 (the latter is shown in the figure). The low-pass filtered

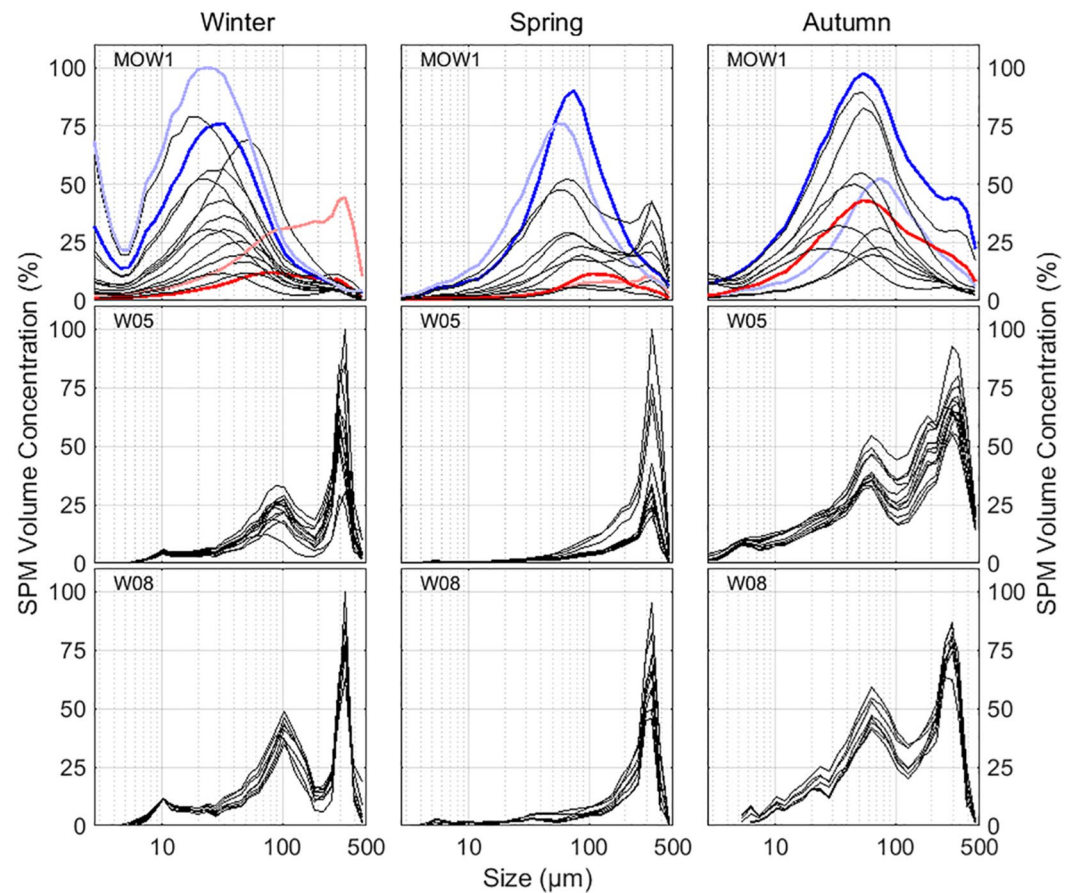


**Figure 3.** Hourly particle size distribution by volume at about 2 m above the seabed during a tidal cycle at stations MOW1 (January, May, and September), W05 (December, May, and September), and W08 (December, May, and September). The volume concentration is normalized by dividing all values with the largest one measured during the tidal cycle. Floc size distribution at MOW1 are highlighted around maximum flood currents (light blue), HW slack (light red), maximum ebb currents (blue), and LW slack (red).

median floc sizes from the long-term LISST measurements (2016–2019) at MOW1 are shown in Figure 4. The median floc size is about 50  $\mu\text{m}$  in winter and increases up to 150  $\mu\text{m}$  in summer. The four-class entropy analysis and the associated mean FSD show a mirrored evolution over the year as a function of seasonal changes. The FSD of class 1 ( $D_{50} = 47 \mu\text{m}$ ) are most prominent between about 15 October and 15 March, those of class 2 ( $D_{50} = 60 \mu\text{m}$ ) in the transitional periods characterized by an increase (15 March to 15 April) or decrease (15 September to 15 October) of biological activity. Class 3 ( $D_{50} = 81 \mu\text{m}$ ) and 4 ( $D_{50} = 116 \mu\text{m}$ ) prevail over spring and summer. The large biomineral flocs ( $>200 \mu\text{m}$ ) are more frequent from late spring till early autumn during the decaying phytoplankton blooms, as indicated by the course in Chl-a.

The FSD by volume (Figure 3) represents the data measured by the LISST. In contrast, the FSD by mass shows the relative importance of the different size classes with respect to mass. The FSD by mass has been calculated following the method presented by Fall et al. (2021) and assuming a primary particle size of 2  $\mu\text{m}$  and a fractal dimension of 2, see Figure B1 (Appendix B). The figure shows that the mass of the particles is concentrated in the smaller size classes in all stations and that the large peaks in volume around 400  $\mu\text{m}$  at W05, W08 and even MOW1 contain particles with a low density. The particles in the smaller size classes contain much of the mineral-associated POC, PON, and TEP. In contrast, the fresh POC, PON, and TEP occur in larger flocs (or particles) having a low density. These particles or flocs dominate, however, the volume distribution in spring and have still a prominent peak in winter and autumn.

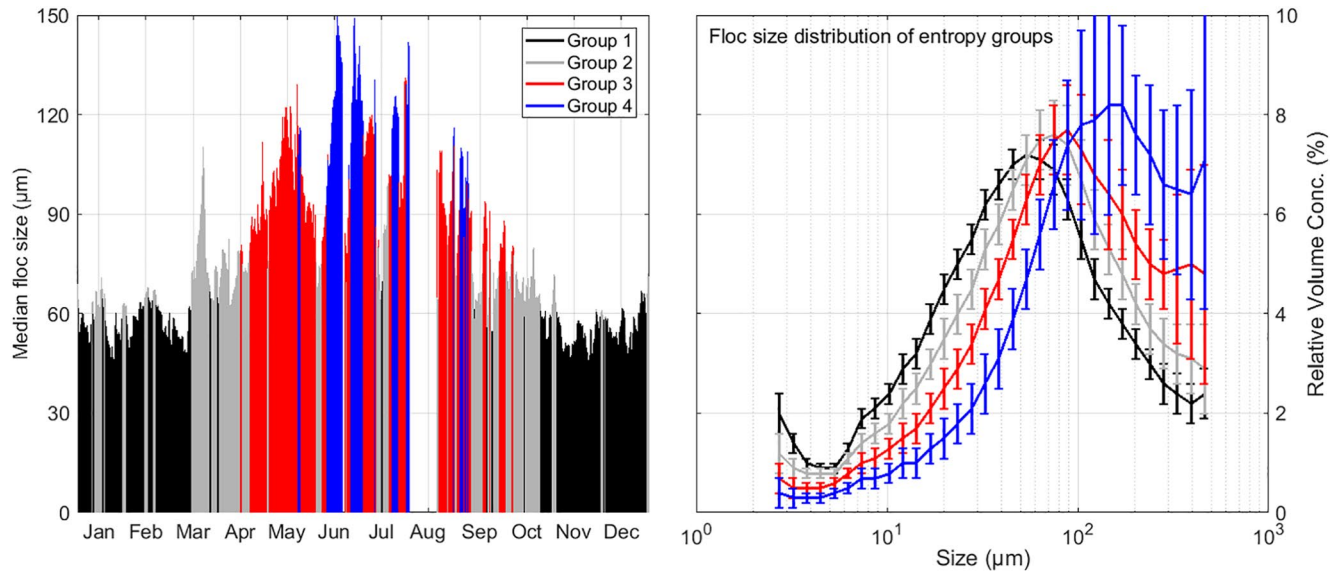


**Figure 4.** Mean of the low-pass filtered median flocculation sizes from the long-term LISST measurements (period 2007–2019) at MOW1 (left). The colors indicate the four entropy groups, the corresponding flocculation size distributions are shown in the right panel.

### 3.3. POC, PON, and TEP Content Along the Coastal to Offshore Gradient

At the basis of the semi-empirical model (Section 2.3), the POC, PON, and TEP content of SPM can be related to the SPM concentration along the coastal-offshore gradient. The POC, PON, and TEP content as a function of SPM concentration for the seasonal sorted data, the surface/bottom sorted data and the data separated by station are shown in Figure 5. Instead of a percentage fraction of SPM, the TEP:SPM ratio is given here in mass units (g XG eq.)/g, because the concentration of the Alcian blue stained microgels cannot be easily related to a mass concentration, for example, of organic carbon, in the presence of resuspended mineral particles. A derivation of a dependency between Alcian blue stained particles and their carbon content at different SPM concentrations is a relevant side aspect of our study (see Appendix C).

The graphs in Figure 5 indicate an increase of the POC, PON, and TEP content with decreasing SPM concentration, which has been documented as a characteristic feature (e.g., Eisma & Kalf, 1979; Fettweis et al., 2006; Jago et al., 1993; Schartau et al., 2019). The figure shows that: (a) a large variability of the data is related to season, (b) the surface and bottom data cannot be distinguished, and (c) the main variation in the data occurs along the transect from the turbid nearshore toward the offshore. The station-sorted data are overlapping as SPM concentration exhibits large variations. SPM concentration at MOW1 can reach low values (<5 mg/l), while the POC, PON, and TEP content for these low values are not distinguishable from those of the offshore stations. This underlines that, although flocculation size and density are different in the nearshore and in the offshore, or vertically (Figures 2 and 3), the POC, PON, and TEP content do not exhibit a spatial signal but a seasonal signal along the range of SPM concentration. In other words, the POC, PON, and TEP content only depends on the SPM concentration and the season.

### 3.4. Model Estimates of POC, PON, and TEP

#### 3.4.1. Yearly Data

Here, we fit the model to all POC, PON, and TEP data. The POC and PON contents of SPM as a function of SPM concentration are shown in Figures 6a and 6b. The fraction of POC contained in the SPM varies between ~2.5% and 30%, while for PON this fraction is clearly lower, ranging between ~0.35% and 4%. From about a 100 mg/l SPM concentration onward the POC and PON content reach an asymptotic value of about 2.5% and 0.35%, respectively. The 10–15 times increase of the POC and PON content occurs over two orders of magnitude in SPM concentration and shows that SPM in the nearshore contains proportionally significantly less OM than in the offshore (see Tables A1–A3 in Appendix A for exact values). The best estimates of  $K_{\text{POM}}$ ,  $f_1$ , and  $f_2$  for annual (all year) representations of POC:SPM, PON:SPM, and TEP:SPM are listed in Table 1. In all cases  $m_{\text{POM}}$  was taken



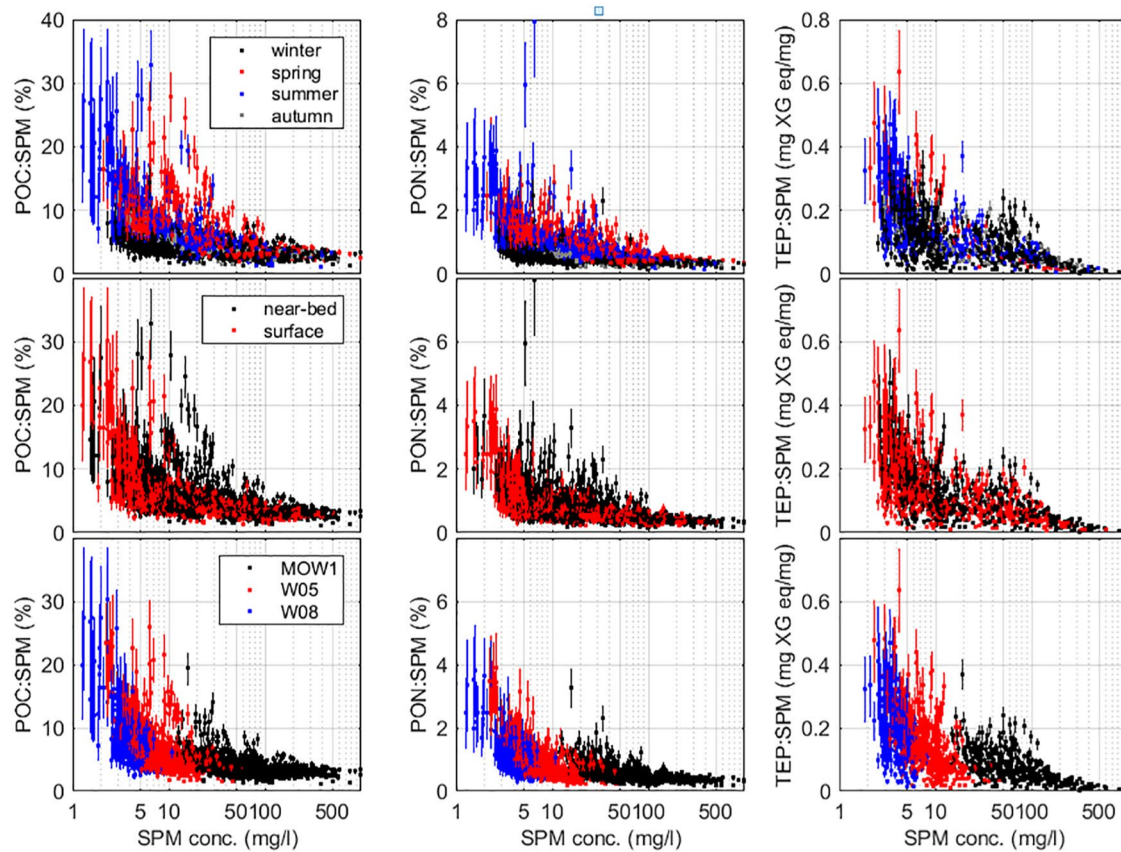


**Figure 5.** Particulate organic carbon, particulate organic nitrogen, and transparent exopolymer particle content as a function of suspended particulate matter concentration. The data are sorted according to seasons (above), surface and bottom (middle), and stations (below).

as the best estimate for the POM model (Equation 4) for the LoI data set from the German Bight and amounts to 0.13 (Schartau et al., 2019).

TEPs incorporate mainly organic carbon. Thus, measured TEP concentrations are not independent of the POC measurements, which is reflected in the significant ( $p < 0.05$ ) correlation between POC and TEP in the data with

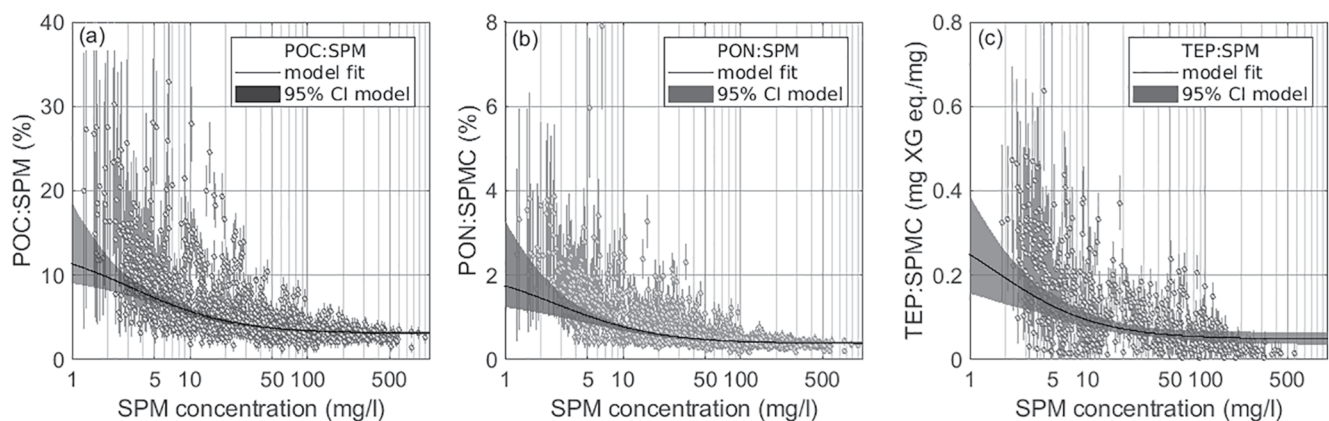


**Figure 6.** Model fit and 95% confidence intervals through all data for the particulate organic carbon content (a), particulate organic nitrogen content (b), and the transparent exopolymer particle content (c) as a function of the suspended particulate matter concentration. The error bars represent the uncertainties of the measurements (see Section 2.2.1). The shaded area is the 95% confidence interval of an ensemble of individual model fits, based on 100 optimizations with different, randomly sampled, data subsets.



**Table 1**  
Model Parameters for POC, PON, and TEP for All Data (Year) and for the Four Seasons

$m_{\text{POM}} = 0.13$	$K_{\text{POM}}$ CI 95% [lower, upper]	$f_1$ CI 95% [lower, upper]	$f_2$ CI 95% [lower, upper]
Year			
POC	3.25 [0.24, 5.53]	0.122 [0.065, 0.981]	0.268 [0.248, 0.291]
PON	2.73 [0.13, 5.75]	0.021 [0.006, 0.203]	0.033 [0.031, 0.036]
TEP	1.61 [0.20, 4.36]	0.367 [0.100, 1.200]	0.422 [0.285, 0.583]
Winter			
POC	3.02 [1.34, 4.49]	0.058 [0.038, 0.112]	0.260 [0.248, 0.273]
PON	3.20 [2.16, 4.22]	0.008 [0.007, 0.011]	0.032 [0.030, 0.033]
TEP	4.25 [2.68, 6.00]	0.097 [0.058, 0.152]	0.251 [0.185, 0.318]
Spring			
POC	4.92 [3.11, 6.70]	0.197 [0.158, 0.261]	0.239 [0.216, 0.258]
PON	4.31 [2.95, 5.61]	0.032 [0.027, 0.038]	0.031 [0.028, 0.034]
TEP	3.67 [2.12, 4.83]	0.489 [0.386, 0.641]	0.457 [0.265, 0.677]
Summer			
POC	2.79 [0.28, 5.40]	0.173 [0.105, 0.993]	0.267 [0.237, 0.306]
PON	2.82 [1.34, 4.05]	0.028 [0.022, 0.043]	0.034 [0.031, 0.039]
TEP	3.27 [1.63, 4.62]	0.379 [0.281, 0.567]	0.456 [0.296, 0.601]
Autumn			
POC	2.18 [0.63, 3.62]	0.141 [0.085, 0.350]	0.282 [0.255, 0.304]
PON	0.90 [0.08, 8.00]	0.033 [0.009, 0.106]	0.031 [0.028, 0.033]
TEP	1.46 [0.10, 10.00]	0.267 [0.020, 1.200]	0.514 [0.392, 0.647]

*Note.* The units for  $K_{\text{POM}}$  are mg/l (same unit as SPM concentration) and for  $f_1$  and  $f_2$  [g/(g POM)] for POC and PON and in [g XG eq./g POM] for TEP. POC, particulate organic carbon; POM, particulate organic matter; TEP, transparent exopolymer particle.

an  $R^2 = 0.59$ . Accordingly, the dependency between TEP and SPM concentration (Figure 6c) is similar to those found for POC and PON (Figures 6a and 6b). The TEP:SPM ratio is approximately 0.05 (g XG eq.)/g at SPM concentrations greater than 100 mg/l. With decreasing SPM concentrations, the ratio increases by one order of magnitude, to  $\sim 0.3$  (g XG eq.)/g at SPM concentrations below 6 mg/l.

### 3.4.2. Seasonally Sorted Data

Our analysis can be refined by sorting the data into their seasonal components. Hence, seasonal values of the model parameters ( $K_{\text{POM}}$ ,  $f_1$ , and  $f_2$ ) can be derived from the model fitting. The annual composite data of POC:SPM, PON:SPM, and TEP:SPM, as depicted in Figure 6, exhibit extensive variability. For the most part, this variability can be attributed to seasonal changes. The fits of the models to annual composite data resolve and explain only differences between the different observational types. Seasonal variations have been further resolved by fitting the models to seasonally sorted data. Table 1 includes estimates of  $K_{\text{POM}}$ ,  $f_1$ , and  $f_2$  all four seasons separately. A higher resolution of temporal changes of parameter values was derived for model fits to TEP:SPM data, with monthly parameter estimates (see Table D1 in Appendix D). In general, the non-linear dependency of the POC and PON content of SPM (Figure 7) varies in a similar way as the TEP:SPM ratio (Figure 8), with clearly altered seasonal signals.

At high SPM concentrations, greater than 100 mg/l, the variability remains small and temporal differences between the model solutions are indistinguishable for POC:SPM and PON:SPM. A large spread in the seasonally resolved model solutions were obtained for TEP:SPM ratio at SPM >100 mg/l (Figure 8). The only noticeable difference is the lower estimate of  $f_2$  obtained for modeling the TEP:SPM ratio at high SPM concentrations in winter. Whether this estimate is actually associated with a clear difference in the mineral-associated fraction of TEP in winter is unclear. Apart from this, the overall spread does not follow any seasonal pattern and must

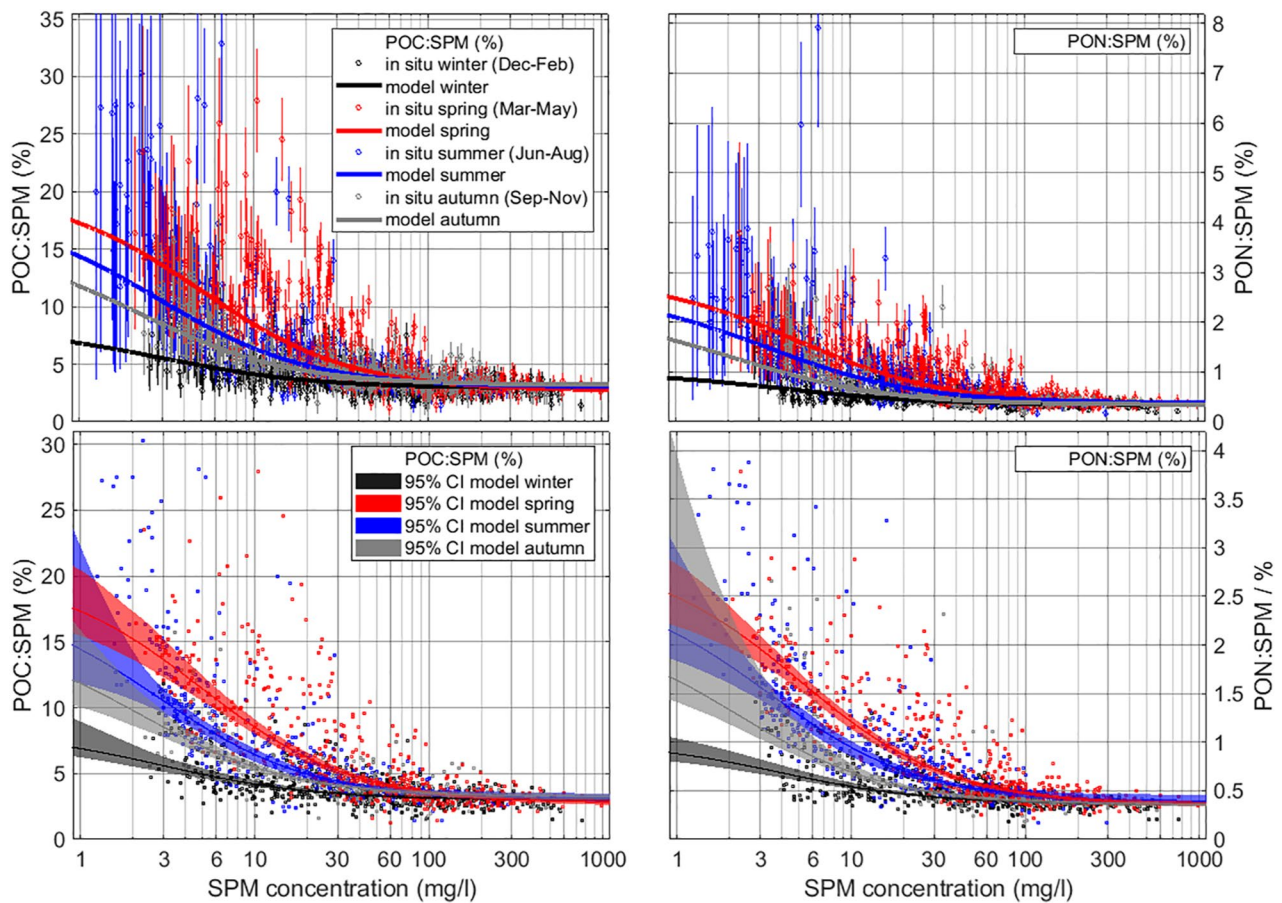


**Figure 7.** Particulate organic carbon and particulate organic nitrogen content (in %) as a function of suspended particulate matter concentration (data from 2004 to 2020). Top panels show the uncertainties of the data as described in Section 2.2.1 and model estimates for the different seasons. Bottom panels show the 95% confidence interval of an ensemble of individual model fits, based on 100 optimizations with different, randomly sampled, data subsets.

be attributed to larger uncertainties in the model fits of the TEP:SPM ratio. Overall, seasonal variations in the mineral-associated fractions of POC, PON, and TEP in SPM could not be identified and appear to be negligible. The small changes may rather be associated with variations in sediment types that contain variable constituents and fractions of minerals.

For SPM concentrations below  $\sim 100$  mg/l, we identified clear and distinctive seasonal patterns. Our results show a correlation with season (and thus with primary production), which is most pronounced in the low-turbid data. In all cases, the seasonal changes could be well resolved (Figures 7 and 8). During the winter season the variations of the SPM's content of POC, PON, and TEP remain small for a large range of SPM concentrations, with only a small increase of respective fractions at low SPM concentrations. The general picture changes drastically for the spring period when phytoplankton blooms induce a substantial increase in the POC and PON content of the SPM, and also the TEP:SPM ratios follow this signal. At SPM concentrations of 1 mg/l, the lower end of the sample values, the POC and PON fractions of SPM are  $\sim 17\%$  and  $\sim 2.5\%$ , and for TEP  $\sim 0.4$  (g XG eq.)/g. During spring the measured POC and PON contents of the SPM feature some high values at SPM concentration between 10 and 50 mg/l, which are not captured by the model solution and are likely caused by the high spatio-temporal variability of patches with elevated phytoplankton biomass concentrations. Still, the model's optimized solutions for spring yield highest in the production of fresh POC, PON, and TEP in this range of SPM concentrations. According to the optimized model solutions, the elevated spring values gradually decrease during summer and autumn, a trend that can hardly be recognized on the basis of the highly scattered sample data alone. The differences between the summer and autumn signals are somewhat less distinctive than their differences to spring conditions. This is because transitional months like September may include a prolonged bloom signal from summer

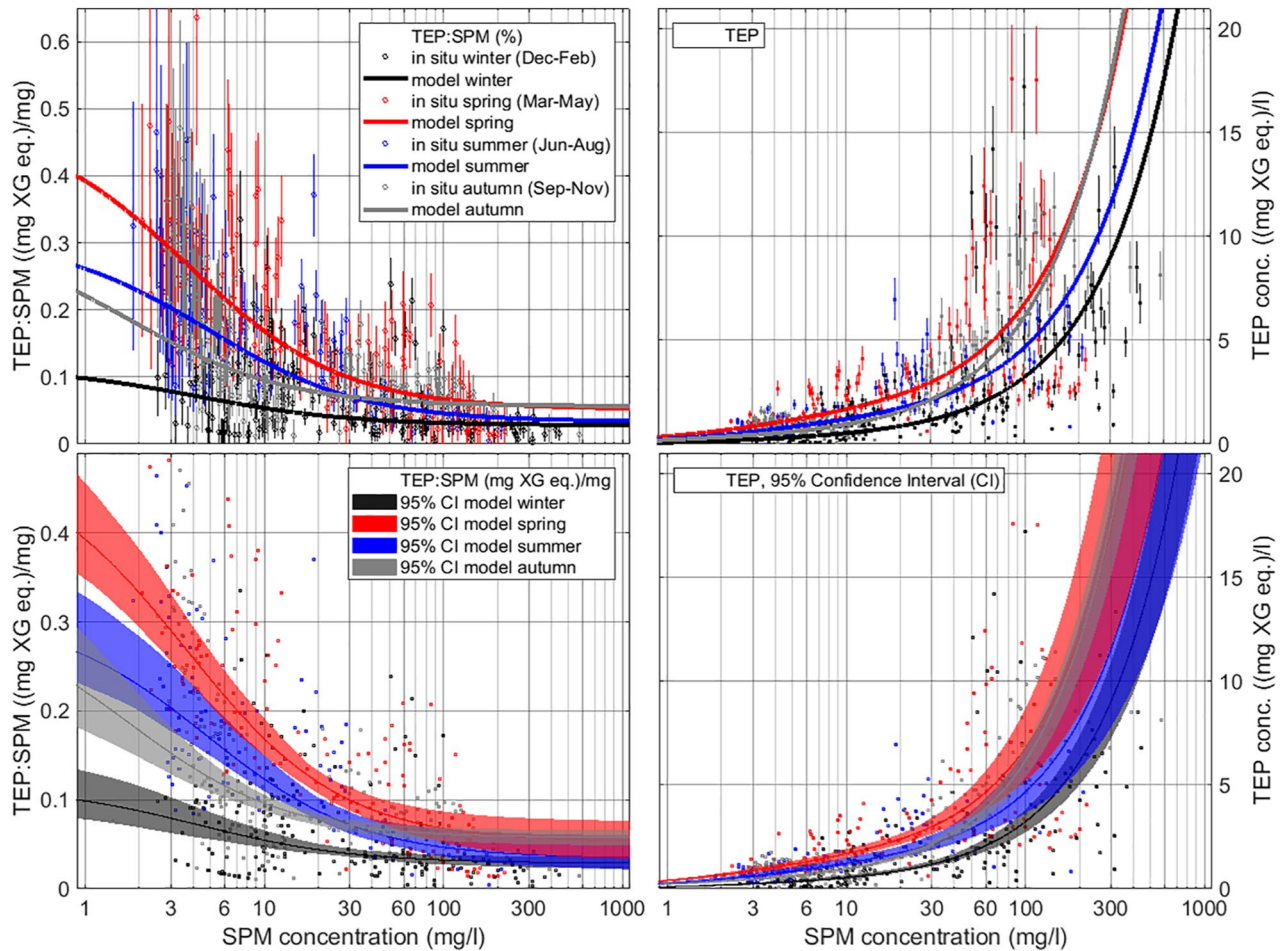


**Figure 8.** Transparent exopolymer particle (TEP) content (left) and TEP concentration (right) as a function of suspended particulate matter (SPM) concentration. The lines are the result of the TEP-SPM model for the different seasons. The error bars represent the uncertainties of the TEP measurements, see Section 2.2.1. Bottom panels show the 95% confidence interval of an ensemble of individual model fits, based on 100 optimizations with different, randomly sampled, data subsets.

or involve secondary bloom events due to the recurrence of elevated nutrient concentrations. The transitions from autumn to winter conditions are again well pronounced.

The ratio  $(f_{1,POC}:f_{1,PON}) = (POC_f:POM_f)/(PON_f:POM_f)$  is indicative for the C:N ratio of the estimated fresh POM ( $POC_f:PON_f$ ), while the same ratio for the  $f_2$  parameter represents the C:N ratio of the estimated mineral-associated POM ( $POC_m:PON_m$ ), see Table 2 and Figure E1 in Appendix E. Both ratios have a seasonal variability, the  $POC_f:PON_f$  ratio compares well with the POC:PON ratio from the observations, which confirms the credibility of our parameter estimates. The winter and autumn values of the fresh  $POC_f:PON_f$  and of the  $POC_{obs}:PON_{obs}$  are above the Redfield ratio ( $6.62 \text{ molN molC}^{-1}$ ) and the summer-spring values below it, but all values agree within the levels of uncertainty. The mineral-associated ratio  $POC_m:PON_m$  is always above the Redfield ratio well beyond the lower 95% confidence limits (except summer), implying that the mineral-associated POM is more enriched in C than the fresh POM.

**Table 2**  
C/N Ratios of the Model Parameters  $f_1(POC):f_1(PON)$  and  $f_2(POC):f_2(PON)$  and of the Ratio  $POC_{obs}:PON_{obs}$  From In Situ Measurements

	$f_{1,POC}:f_{1,PON}$ CI 95% [lower, upper]	$f_{2,POC}:f_{2,PON}$ CI 95% [lower, upper]	$POC_{obs}:PON_{obs}$ CI 95% [lower, upper]
Winter	7.99 [4.35, 16.15]	8.39 [7.78, 8.98]	7.67 [5.27, 11.99]
Spring	6.85 [5.12, 9.14]	7.81 [6.80, 8.83]	7.13 [5.14, 10.19]
Summer	7.37 [1.41, >20]	8.06 [6.43, 9.95]	6.76 [4.99, 10.33]
Autumn	5.42 [2.66, >20]	9.12 [8.31, 9.96]	7.64 [5.11, 12.76]

#### 4. Discussion

The main objective of the study is to unravel compositional changes of SPM and relate them to the seasonal buildup and breakdown of flocs in coastal oceans. For this, we applied data-model syntheses and investigated the explanatory power of our model-based separation of POC, PON, and TEP into

respective fresh, rather labile, fractions and their mineral-associated, more recalcitrant, fractions. In principle, flocculation depends on a number of local environmental conditions, for example, turbulence, cation concentration, SPM concentration as a proxy particle number density, mineral composition, POM concentration and composition (e.g., TEP) and microorganism (Dyer, 1989; Keyvani & Strom, 2014; Lai et al., 2018; Manning et al., 2010; Mietta et al., 2009; Zhang et al., 2021). The bulk mineralogical composition of the SPM in the study area is relatively constant and consists of 32%–39% clays, 25%–33% carbonates, 12%–18% quartz, 11%–15% amorphous silicates, and 5%–8% feldspars and accessory minerals (Adriaens et al., 2018). The cation concentrations are high and well above the threshold for salinity induced flocculation so that flocculation in the study area is above all controlled by the OM composition of the SPM, the SPM concentration and the hydrodynamic conditions. The effect of turbulence and SPM concentration on flocculation in the study area has been described in previous studies (Fettweis & Baeye, 2015; Fettweis et al., 2006, 2014). They reported that maximum floc size was mainly controlled by turbulence intensity (tides and waves), which is higher in the nearshore area than offshore, but does not exhibit a pronounced seasonal signal. Our LISST data (Figure 3) confirm that the size of the largest flocs is similar during all seasons, but their abundance is higher in spring and summer, because they seem to be more tightly bound and resist better shear-induced breakup.

The seasonal dependence of SPM concentration with lowest values in summer (Figure 2d) contrasts with the inverse dependence of the median floc sizes being highest in summer (Figure 4, left panel). Thus, SPM concentration in itself can be ruled out to explain flocculation and the qualitative properties of SPM may provide a much better clue. Given the large variability in SPM concentration within the nearshore areas and along the transition to the offshore waters, the spatial and temporal changes in SPM composition may unravel predominant variations involved in the processes of flocculation. In the following we will discuss how the modified application of the POM-SPM model of Schartau et al. (2019) to the POC, PON and TEP sample data turned out to be beneficial. With the aid of the calibrated model solutions we could estimate how the relative fractions of freshly produced labile and semi-labile OM (of POC, PON, and TEP) along with the rather recalcitrant mineral-associated OM content of the SPM change with SPM concentration. A starting point of this approach is the obvious concurrence of seasonal rises and declines in median floc size (Figures 3 and 4) with estimates of the model parameter  $K_{\text{POM}}$ , which reflects the seasonal buildup of fresh organic material and its components (Figures 5–8 and Table 1). Our syntheses between model application and in situ measurements deliver important insight into the complex process of flocculation in a region of great variability. Based on results of our analyses we can expand the scope of discussion on how the fresh and the mineral-associated OM fractions of the SPM affect the process of biophysical flocculation.

#### 4.1. Spatio-Temporal Variations of Floc Characteristics

Flocs in the nearshore high turbid station MOW1 were subject to extensive temporal variations in volume concentration, density and size during a tidal cycle (Figures 2 and 3). The FSDs were skewed toward smaller sizes around peak flow (blue in Figure 3) and developed a peak in the larger size classes around slack water (red in Figure 3). B. J. Lee et al. (2012) have shown that the flocs at MOW1 are characterized by a multimodal size distribution that consists of small particles, flocculi, microflocs, and macroflocs. The smallest particles likely consist of clay-sized particles of various mineral composition, the flocculi are breakage-resistant aggregates of clay minerals. Microflocs can be attributed to the medium size aggregates, whereas macroflocs can be identified as the large aggregates with diameters up to a few hundred micrometers. Tran and Strom (2017) have shown in a laboratory experiment that silt and clay combine into flocs, other studies described the flocculation of sand-mud mixtures (Manning et al., 2010). In some contrast to this, we observe (Figures 3 and 4) that the FSDs at MOW1 all had well pronounced modes within the smallest size classes in winter. This mode diminished toward summer. This indicates that in winter abundant fine-grained mineral particles do not aggregate into larger flocs. They settle slowly and remain in suspension longer, resulting in a background turbidity that is higher than in summer. In general, lower turbulence intensities before slack water promote the aggregation of the more mineral flocculi (i.e., with a POC content of about 2.5%) and of microflocs that form larger macroflocs. In winter these macroflocs have similar characteristics than the microflocs, that is, they are mineral enriched (Tang & Maggi, 2016). In summer, the small particles, flocculi and microflocs also coagulate with freshly produced OM to form stable and sticky aggregates that are enriched with biogenic substances, including phytoplankton cells and detrital substances. These spring and summer flocs have lower densities than the winter and autumn flocs (see Figure 2g and Tables A1–A3 in Appendix A) but reach floc sizes that involve settling velocities that exceed those of the smaller



winter flocs, which leads to their accumulation near the bed and thereby reduces the average SPM concentrations in the water column.

In contrast, in the offshore stations W05 and W08, the seasonal variabilities in the concentration of SPM and the OM parameters seem less pronounced and the FSD remains rather similar over the tides (Figure 3), revealing how aggregation dominates disaggregation kinetics (Fettweis & Lee, 2017). The principal variations in these parameters occurred between seasons and not within tides. In winter and autumn, the FSDs were multimodal, with a first mode around 10  $\mu\text{m}$ , a second one around 50–100  $\mu\text{m}$ , and a third one around 300  $\mu\text{m}$  (Figure 3). The first mode could consist of flocculi, while the second mode could be formed by minerals from biogenic origin (carbonates, amorphous quartz). In spring, the 300  $\mu\text{m}$  peak dominated the FSDs. In summer, the increase of the median floc size in these offshore stations (see Figure 2) indicates that the observed decrease of the lower modes is caused by the incorporation of these particles into the larger aggregates. These larger biological aggregates can be lighter and even settle slower than smaller bio-mineral aggregates found at MOW1 (Maggi & Tang, 2015).

## 4.2. TEP Concentration and Its Relation to Floc Size

### 4.2.1. Seasonal Variation in TEP Concentration

A correlation of TEP concentrations with the rise and decline of phytoplankton blooms is reported from lab cultures (Fukao et al., 2010), estuarine and nearshore areas (Bhaskar & Bhosle, 2006; Chowdhury et al., 2016; Ramaiah et al., 2001), and from the open ocean (Mari et al., 2017). Others report temporary disconnection of TEP from Chl-a concentrations (J. H. Lee et al., 2020; Ortega-Retuerta et al., 2018). Our data do not reveal any clear relationship between Chl-a and TEP concentration (see Figures 2j and 2l). The decorrelation can be explained by TEP observed at times of extensive resuspension (e.g., winter period) to have biogeochemical properties that differ from TEP measured during spring and summer, at times of little resuspension. Our results indicate the occurrence of two types of TEP, presumably having different chemical characteristics with respect to their stickiness and their potential to promote the formation of flocs of large size. In the shallow nearshore station MOW1 a substantial fraction of TEP appears to be rather mineral-associated, entering the water column via resuspension of sediment particles. At MOW1 the TEP concentration followed the SPM concentration irrespective of the season, including winter when primary production has largely ceased (Figures 2d and 2j and Figure 8, right panel). This general dependency is modulated by a seasonal signal, depending on the amount of OM being built up via primary production. It is this seasonal signal that can be expected to disclose some correlation between Chl-a and TEP.

Our seasonal pattern is in line with findings from the turbidity maximum of the Seine estuary (Morelle et al., 2018). There, the highest TEP concentrations coincide with the lowest EPS and DOC concentration in winter and vice versa in summer. In contrast, the more offshore stations, where SPM concentration remained most of the time below 10 mg/l, had TEP and POC concentrations that were generally higher in spring and summer than in winter. The offshore environments with low turbid conditions agree with the correlation found by Mari and Burd (1998) between DOC and TEP concentrations suggesting that TEP are formed by coagulation of the dissolved EPS (Engel et al., 2004; Mari & Burd, 1998).

An obvious dependency between total abundance of TEP and floc size cannot be inferred from our data. The interpretation of the results for the station MOW1 is complicated, in particular because similar TEP concentrations were concomitant with different floc sizes in winter and summer (see Figures 2f and 2j). Morelle et al. (2018) have explained the higher TEP concentration in winter by deposition and resuspension processes, which implies that, due to the larger flocs in spring and summer, a large part of TEP is found in the benthic boundary layer or on the bed exclusively, and in winter it becomes resuspended. Such interpretation is incomplete, since it does not explain why floc sizes were found to be smaller in winter, supported by studies relating floc size to TEP concentration (e.g., Deng et al., 2019; Passow, 2002) and by our data. Our analysis suggests that biophysical flocculation in highly turbid areas is strongly affected by the occurrence of fresh OM rather than the total amount of OM. Amongst the fresh OM are TEP, whose production rapidly increased when the maximum capacity for the build-up of fresh POC and PON was reached (Figure 9). The maximum rate of TEP formation occurs shortly after phytoplankton have exuded excessive organic carbon in form of carbohydrates, at times when the intracellular carbon cannot be allocated for growth, for example, under conditions of nutrient limitation (Engel et al., 2004; Schartau et al., 2007). We could not explicitly resolve the process of TEP formation from dissolved precursors, but found generally higher DOC concentration in spring and summer, which is likely associated with the production of



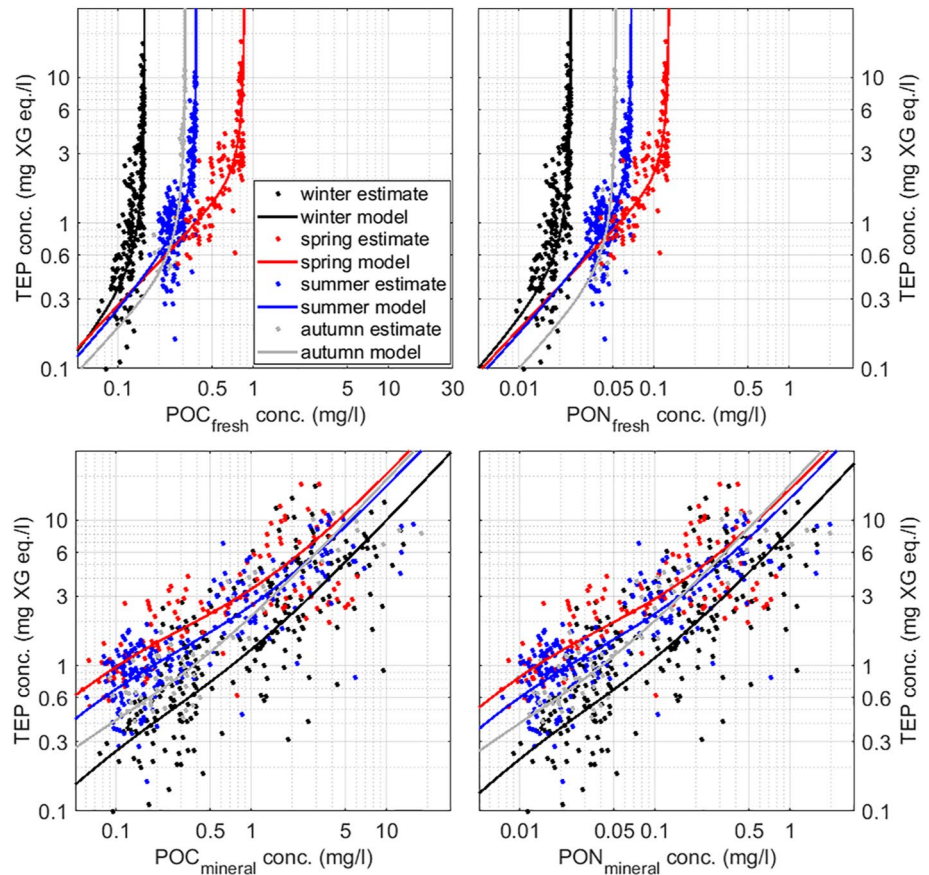


**Figure 9.** The observed total transparent exopolymer particle (TEP) concentration versus the model derived fresh (upper panel) and mineral-associated (lower panel) particulate organic carbon (POC) and particulate organic nitrogen concentration. The lines are the estimated total TEP concentration as a function of POC and PON concentration derived from the POM-suspended particulate matter model.

dissolved combined carbohydrates by algae and bacteria. Figure 2k shows that the concentration of DOC, which comprises EPS, has a maximum in late spring and summer, as in the Seine estuary (Morelle et al., 2018).

To assess the relationship between the time evolution of SPM and TEP in their quantities and qualities, Figure 10 shows the low-pass filtered median floc size data at the high turbid station MOW1 (as in Figure 4) together with the low-pass filtered long-term SPM concentration time series (upper panel), as well as the seasonal evolution of fresh and total TEP concentration (lower panel) derived from calibrated results of the TEP-SPM model based on monthly model parameter estimates of  $K_{POM}$ ,  $f_1$ , and  $f_2$  (Appendix D). When fresh TEP is produced (from half February onward), the median floc size increases (in particular from March on, when the proportion of fresh TEP to total TEP ratio increases) and SPM concentration decreases. Although fresh TEP concentration is at its maximum in early spring, the increase in median floc size, the changes in FSD (Figure 4) and the decrease in SPM concentration occur more gradually. The progressive rise in floc size follows the increase and the decrease of the fresh TEP fraction ( $TEP_{fresh} : TEP_{total}$ ). This ratio is low during winter (about 2%) and starts to increase from the beginning of February to about 15% in March and then more quickly to reach a maximum around 60% in May-June. The peaks in floc sizes as well as the lowest SPM concentrations were observed during this period.

The decrease of the fresh TEP concentration after its quick accumulation in spring occurs gradually over a period of about 6 months (May-November) and can be due to hydrolyzation, consumption and/or deposition. This is in contrast with the early spring period, where most of the fresh TEP accumulation occurs within about 1 month (February-March), before reaching a maximum in early May. The production of fresh TEP correlates with the first increase in Chl a concentration in February in 2019 and the first decrease of SPM concentration from the beginning of March onward (MOW1, Figures 11a). These findings support the hypothesis that in early spring in the

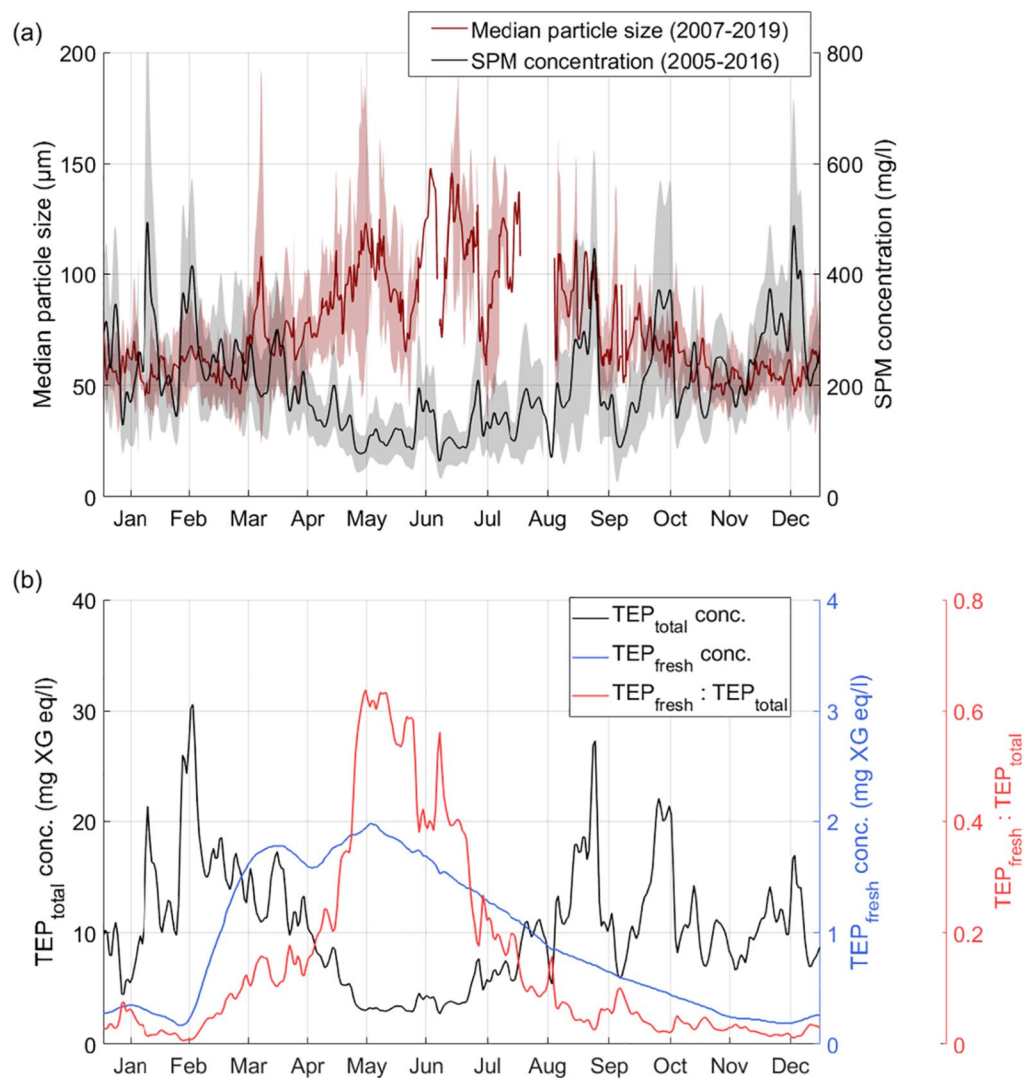


**Figure 10.** (a) Long-term and low-pass suspended particulate matter concentration (2005–2016) and median floc size (2007–2019) at 2 m above bed. The shaded area is the standard deviation if more than two data points are available. (b) The model estimates of total (black) and fresh (blue) transparent exopolymer particle (TEP) concentration calculated from the long-term SPM concentration time series. The red line is the fraction of fresh TEP in the total TEP. All data are from the near shore station MOW1.

turbid nearshore, when light conditions are still depleted, light adapted phytoplankton species initiate the spring bloom and also induce the formation of fresh TEP. In contrast to the mineral-associated TEP, it is this initial occurrence of fresh TEP that eventually promotes aggregation and the formation of larger flocs with higher settling rates. This in turn lowers SPM concentration and reduces light attenuation, which paves the way for species with higher light requirements in the phytoplankton seasonal succession.

In the intermediate station, W05, the SPM concentration was higher in winter ( $>20 \text{ mg/l}$ , Figures 11b) and the TEP concentration had also a maximum (Figure 2j). The spring phytoplankton bloom correlates with an increase in the TEP and the decrease in SPM concentration to values about  $5 \text{ mg/l}$ . Similar observations are from the offshore station W08 (Figure 11c), although less pronounced as W05. Altogether, the results underline that the different components of the SPM (i.e., mineral, OM, and living particles) form an integrated dynamic system with direct interactions and feedback controls.

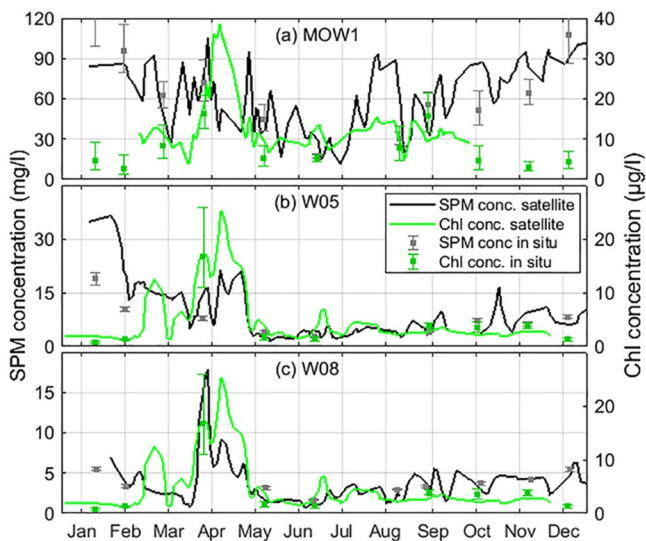


**Figure 11.** Time series of surface suspended particulate matter and Chl-a concentration in 2019 derived from remote sensing (Sentinel-3/OLCI) and in situ observations at station (a) MOW1 (nearshore), (b) W05 (intermediate), and (c) W08 (offshore). The in situ data are mean values over a tidal cycle, the error bars are the standard error of the mean.

#### 4.2.2. TEP in Autumn and Winter

What are the quantitative and qualitative characteristics of TEP outside the growth season? The presence of high concentrations of TEP in autumn and winter above all in the turbid nearshore (Figure 2k) raises questions on the characteristics of this OM. Mari et al. (2007) mention that the efficiency of the transformation of dissolved EPS into TEP and the TEP reactivity decrease with time. This would mean that the TEP stickiness varies as a function of the degradation stage and age. Winter TEP would then be smaller in size and less sticky, while in spring and summer it would consist of larger and more sticky particles that become actively involved in flocculation dynamics (Engel et al., 2020). The biomineral flocs resist better to shear-induced break-up in spring and summer due to availability of more reactive TEP and of the inclusion of free-floating bacteria and other microorganisms into the flocs that produces themselves exopolymers (Fettweis et al., 2014; Jachlewski et al., 2015; Shen et al., 2019). The bacteria associated with TEP contribute to the hydrolysis of the OM and thus foster the gradual decay and disaggregation of the biomineral flocs in autumn (Alldredge et al., 1993; D. C. Smith et al., 1992; Passow & Alldredge, 1995), which is reflected in the observed decrease in floc size in our data. As the transition from summer to winter is gradual, one would expect that TEP concentration decreases through microbial respiration until a minimum is reached just before the onset of the algae bloom in early spring. The latter is observed in the low turbid offshore stations W05 and W08, but not in the turbid MOW1 station, see Figure 2j. Other studies highlight the relationship between OM content and

mineral surface area (Keil et al., 1994; Mayer, 1994). This means that with increasing SPM concentration, the OM concentration and thus also TEP concentration increases, while the POM content of the SPM decreases until reaching an asymptotic value at high SPM concentrations (>100 mg/l) of about 2.5% POC, 0.4% PON, and 0.04 (mg XG eq.)/l TEP (Figures 5–8). At high SPM concentrations the fresh OM represents only a small part of the total OM and is hardly detectable due to the high variability of the measurements. Both the fresh and refractory OM can be associated to the mineral surfaces, being protected from microbial respiration (Chen et al., 2021; Hemingway et al., 2019; Kalbitz et al., 2005; Keil et al., 1994). The protected mineral-associated OM explains the high TEP concentrations in winter in high turbid areas such as the Belgian nearshore, Chesapeake Bay (Malpezzi et al., 2013) or the Seine estuary (Morelle et al., 2018).

The mineral-associated POC over TEP ratio is about 1 in winter and between 0.52 and 0.59 (mean 0.56) during the other seasons (see Appendix C). The higher ratio in winter is the result of the optimal estimation of the POC and TEP content in the SPM based on our data. The model estimates a lower value of the TEP content in the SPM in winter at high SPM concentrations than for the other seasons (Figure 7). Such distinction could be explained by a lower amount of mineral-associated TEP in winter and by the occurrence of two different mineral-associated TEP fractions. One is more recalcitrant and remains, while the other one is still subject to gradual but slow degradation and eventually disappears in winter. The first one could consist of the TEP that occurs in between the layers of the clay crystal structures (Blattmann et al., 2019; Mayer, 1994). The second one could consist of a semi-labile biofilm on the surface of the mineral particles (Decho & Gutierrez, 2017). Anyway, the mineral-associated POC over TEP ratios indicates that the recalcitrant mineral-associated TEP makes up a great portion of the mineral-associated POC.

To conclude, while also present during autumn and winter, fresh TEP occurs at much lower concentration then. It could originate from winter biological activity, from bacteria or phytoplankton (Chl-a concentration in winter is on average between 1.1 µg/l at W08 and 3.5 µg/l at MOW1, see Appendix A). The flocs in autumn and winter can thus be considered as biophysical in nature as few fresh TEP is available to aggregate cohesive particles (such as clay minerals) with non-cohesive ones (such as carbonates) into larger floc. The rising tails in the winter FSD at MOW1 (Figures 3 and 4) point to the occurrence of particles smaller than the measuring range of the LISST (i.e., 2.72 µm) and indicate that the efficiency of biophysical aggregation in winter is, however, much lower than in spring and summer in the high turbid nearshore.

### 4.3. Spatial Variation in SPM Composition

#### 4.3.1. Asymptotic Decrease of OM Content With Increasing SPM Concentration

The surface sediments at W05 and W08 consist of medium sand with small amounts of fines (a few %) and POC contents in the fraction  $<63 \mu\text{m}$  of about 1.8% and 1.1%, respectively. These values are lower by a factor of 4 and 8, respectively, than the mean POC content of the SPM in these stations (see Tables A2 and A3 in Appendix A). In these stations the SPM concentration was generally below 10 mg/l and the seabed consist of medium sized sand. This is a clear indication that the suspended material can only to a minor part originate from the sea bed and illustrates nicely the increasing decoupling of near bed and water column processes with water depth and distance from the coastline (Malarkey et al., 2015). In the nearshore station MOW1, the amount of the fraction  $<63 \mu\text{m}$  in the sediments is about 50% (Fettweis & Van den Eynde, 2003), the POC content of the surface sediments (fraction  $<63 \mu\text{m}$ ) is only lower by a factor of 1.25 than of the SPM at high concentrations (2% vs. 2.5%) and indicates that the surface layer of the seabed is actively involved in the tidally induced resuspension and deposition of the particulate material (Table A1 in Appendix A). The asymptotic value of 2.5% POC at high SPM concentration shows that the minerals are saturated and that no long-term accumulation of OM occurs in the nearshore station MOW1. The fresh OM that is not associated with the mineral surfaces will thus quickly be consumed in the food web. Similar values of the POC contents of the SPM have been found in the turbidity maxima of the Seine and Loire estuary (Etcheber et al., 2007), lower ones in the Gironde estuary (Etcheber et al., 2007) and higher ones in the Yangtze (Milliman et al., 1984) and Congo river (Bouillon et al., 2012). It is remarkable that these variations in POC content between different areas are relatively small (2%–5%), which points to a similar composition of the SPM in many turbid aquatic ecosystems over the world. The small differences are probably caused by methodological differences, measuring uncertainties and by different mineral-associations of the SPM, as the preservation of OM is controlled mainly by its clay mineralogy (Blattmann et al., 2019).

#### 4.3.2. Nearshore to Offshore Gradient in Fresh and Mineral-Associated OM

We used the Sentinel-3/OLCI satellite images of SPM concentration to extract the cross-shore variation of mineral-associated and fresh components of POM, POC, PON and TEP at the water surface. Taking the model parameters for  $f_1$ ,  $f_2$ ,  $K_{\text{POM}}$ , and  $m_{\text{POM}}$  (see Table 1), we applied the model pixelwise to the remote sensing data. In this way, we generated eight further secondary satellite products purely based on SPM surface concentration. For the purpose of this study, we discuss these data for all seasons along a transect the connects the three measuring stations from the coast (MOW1) with SPM concentration  $\cong 80 \text{ mg/l}$  via W05 to the offshore (W08) with  $\cong 2 \text{ mg/l}$  (see Figure 12).

The mineral-associated part (middle) follows to a large part the SPM concentration and has the same strong decrease with increasing distance from the coast. The fresh POM (left) in contrast, nearly keeps his level along the whole transect. The major seasonal formation of fresh POM thus occurs not only within the shallow coastal regions but extends along the whole area. These patterns are similar for all components of the POM and TEP and for all seasons. For the mineral-associated parts, winter has the highest and summer the lowest values except for TEP where the highest values are during the periods of spring and autumn blooms. The fresh parts are always highest in spring and lowest in winter. The ratios of fresh to mineral-associated POC, PON, and TEP (right) show that there is a zone somewhere around station W05, where both fractions are about equal (ratio = 1). This may be identified as a transition zone where, seen from the land, the near coast conditions with particle dominance from the sea bed turn into open sea conditions with particles who are of pelagic origin. This transition zone is located in between MOW1 and W05 in spring and summer at a water depth around 15–20 m and corresponds with a surface SPM concentration of about 40 mg/l in spring and about 20 mg/l in summer. It is located more offshore in autumn where it occurs around W05 (water depth around 20 m) with about 8 mg/l SPM concentration and close to W08 in winter.

#### 4.3.3. Validity of the Model in a Larger Area

In general, we learned that the results from the BCS (Southern Bight) and from the German Bight (Schartau et al., 2019) are qualitatively very similar, although fine-grained sediment dynamics in a larger area, such as the North Sea, can be complicated by the multitude of local and remote sources, transport routes and sink. What is the validity of such a model for a larger area? Our semi-empirical POC, PON, and TEP model is based on data that have been collected in the Southern Bight of the North Sea and uses the assumption that the value of the parameter  $m_{\text{POM}}$  from the German Bight (Schartau et al., 2019) is also valid here. Our estimates of the mineral-associated



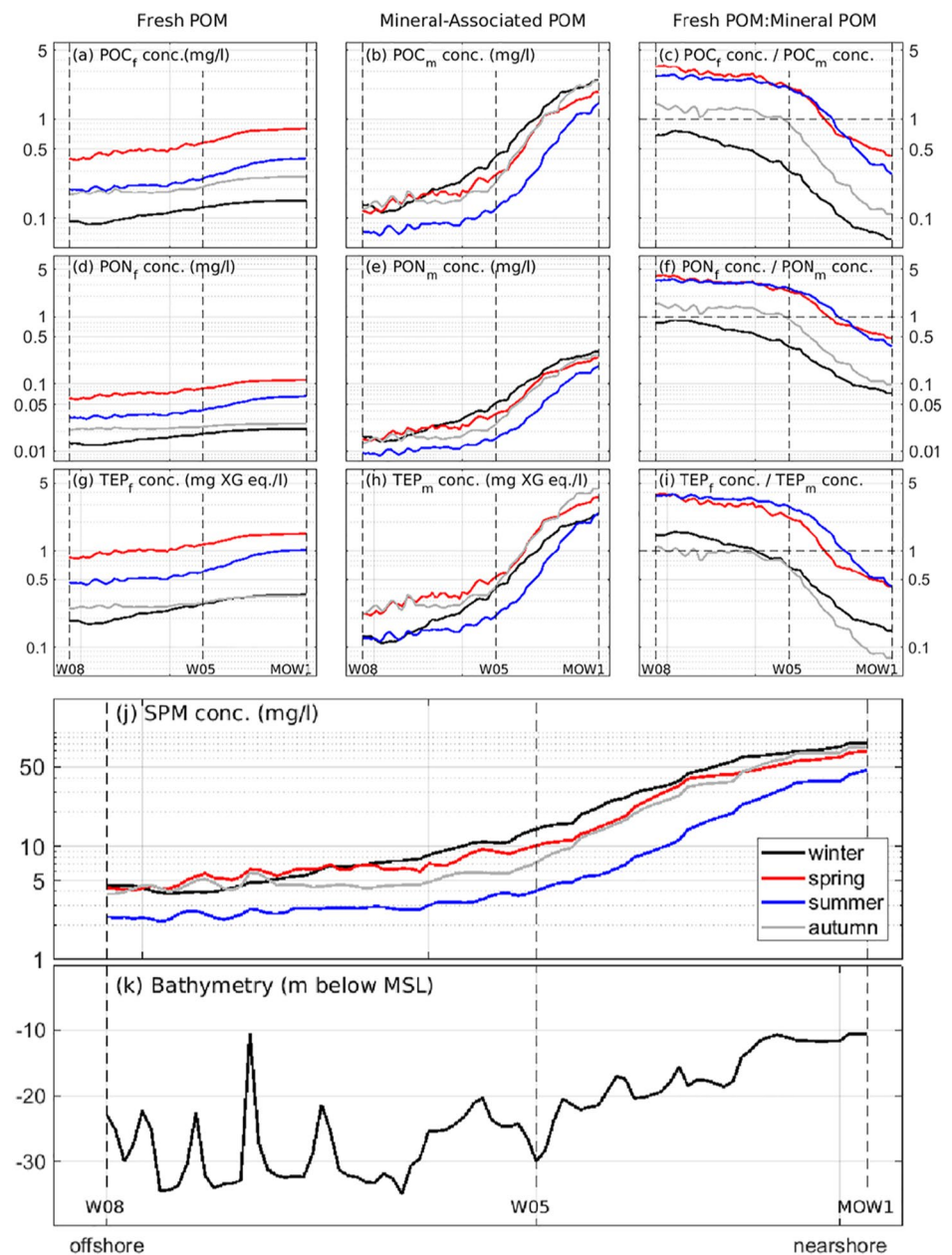


**Figure 12.** Model estimates of the nearshore (MOW1) to offshore (W08) fresh (left column) and mineral-associated (middle column) particulate organic carbon (POC) (a and b), particulate organic nitrogen (PON) (d and e) and transparent exopolymer particle (TEP) (g and h) concentrations calculated from the Sentinel-3/OLC derived surface suspended particulate matter concentrations (j) using the model parameters of Table 1. The right column shows the ratios of fresh to mineral POC (c), PON (f), and TEP (i) concentration. Values above 1 have a fresh POC, PON, or TEP concentration that exceed the mineral-associated one. The lower panel (k) shows the bathymetry (m below mean sea level) along the transect. The large changes in bathymetry between W05 and W08 are from sandbanks.

POC, PON, and TEP depend on this assumption.  $m_{\text{POM}}$  is largely determined by the nature of the mineral particles, more specifically the amount and types of clay minerals in the SPM and may thus be different at other locations (Blattmann et al., 2019). Specifically, the clay mineralogy and content of the SPM are known to vary and are subject to changes in the North Sea (Adriaens et al., 2018; Pache et al., 2008; Zuther et al., 2000). However, as the prior estimates of  $m_{\text{POM}}$  of Schartau et al. (2019) were obtained by combining samples from a variety of different German Bight sediment types, we consider the value of  $m_{\text{POM}} = 0.13$  as a robust mean value that is representative for coastal areas of the southern North Sea.



The seasonal buildup of fresh POC, PON, and TEP can be described as a saturation function of the SPM concentration with a parameter  $K_{\text{POM}}$  that varies with the amount of fresh POC, PON, and TEP being produced, which is inversely correlated with nutrients. Nutrient concentrations not only change with season but also with the distance from the coast and with the eutrophication status (Desmit et al., 2018, 2020; Rousseau et al., 2002). We stress that values of the parameter  $K_{\text{POM}}$  can only be constrained if data from high turbidity locations are combined with offshore measurements, thereby covering a wide range of SPM concentrations. With data from areas that do not yield a wide range of SPM concentrations, the estimates of  $K_{\text{POM}}$  can become deficient and the model should be applied to a (surrounding) larger area with caution. Apart from the range of SPM concentrations covered by the data used for model calibration, the estimates of  $K_{\text{POM}}$  should be representative for a larger area within which the eutrophication status remains similar. Notwithstanding the possible variabilities of the model parameters in a larger area, the seasonal variations and the location of the transition zone at a water depth of about 20 m suggests that the model is informative and sufficiently robust to be applied, at least in a qualitative way, to a larger area.

#### 4.4. Consequences for the Modeling and Monitoring of Coastal Ecosystems

Changes in coastal ecosystems are often correlated with changes in water clarity or SPM concentration and thus with the POM content of the SPM (e.g., Capuzzo et al., 2015; May et al., 2003). The composition of SPM is the result of multiple natural processes that reflect the continuous mixing of marine and terrestrial particles of various ages and origins over geological time scales (Adriaens et al., 2018). Also, human activities have impacted the SPM concentration and composition. While the strongest anthropogenic changes in the study area occurred during the last decades, human occupation and landscape development date back to the last two millennia. They inevitably have had an impact on SPM composition and concentration (Baeteman et al., 2002). In the last decades, the North Sea has been subject to changes in SPM concentration and biological activities amongst which are the decrease in phytoplankton production and changes in community structures (Capuzzo et al., 2018; Nohe et al., 2020); the shift in chlorophyll a phenology (Desmit et al., 2020); the imbalance in the biogeochemical cycles of nutrients (Desmit et al., 2018; Rousseau et al., 2002); and the increase of the SPM concentration due to major construction works (Hendriks et al., 2020; van Maren et al., 2015).

The area where the concentration of fresh and mineral-associated POM is about equal is of particular interest. For the German Bight, this transition zone is typically found at water depths of approximately 15–20 m along cross-shore transects and is characterized by a maximum of the settling velocities (Maerz et al., 2016). Human activities, for example, dredging and dumping operations in the turbid nearshore, wind farms in the low turbid offshore areas or the effect of global warming (Baeye & Fettweis, 2015; Fettweis et al., 2012; Høyer & Karagali, 2016; Jaiser et al., 2012) might influence the localization of this transition zone and could make it a key element in monitoring programs such as the EU Marine Strategy Framework Directive. With our data-model syntheses we could consolidate a relationship that can be applied to SPM concentrations derived from other sources, for example, from in situ long-term observations using optical and acoustic sensors or from remote sensing. A good example for such an application was documented by Schartau et al. (2019) for resolving spatio-temporal variations in fresh and mineral-associated fractions of POM in the German Bight. Though still imperfect, the application of the refined model to satellite SPM concentration products or high-resolution in-situ time series of calibrated optical or acoustical instruments will yield spatio-temporal compositional changes of the SPM, with respect to POC, PON, and TEP, both on large scales and for anomalous events. This greatly facilitates the monitoring of water quality parameters along the gradient from a domination of mineral-associated OM toward a domination of fresh OM, as documented in Figures 10 and 12, and enhances its information content without the increase of resources.

Many oceanographic quantities are often inaccessible to direct observation, due to the high cost of in situ sampling, the limitation of the standard water quality parameters and the low spatial and time resolution. Proxies, based on automated, highly resolving instruments are valuable as they help to extend undersampled or unobserved parameters. In this regard, SPM concentration as a proxy for POM, POC, PON, and TEP concentrations seems to be a key ingredient for the assessment and calibration of numerical models of coastal waters, ranging from SPM transport and deposition to key ecosystem processes.

Specifically, we have shown that the FSD depends on the SPM concentration and on the availability of fresh TEP. In areas where the fresh over mineral-associated TEP is about unity and the SPM concentration low, flocculation occurs on a seasonal time scale rather than a tidal one (Figure 3). In high turbid environments, flocculation occurs on both a tidal and seasonal time scale (Figures 3, 4 and 10). Our model-based differentiation between fresh and

mineral-associated POC, PON, and TEP shows, that SPM concentration can be used as a proxy of the flocculation kinetic model parameters (i.e., break-up and aggregation) adopted in numerical SPM transport models.

## 5. Conclusions

The relevant processes and the critical parameters that drive the mutual interactions between sediment and biological dynamics occur on a wide range of spatial and temporal scales. The OM content of the SPM is highly variable due to physical processes, such as tides and waves, varies with season due to biological activities and with the SPM concentration. There is a distinct difference between the offshore, more open ocean, and the turbid nearshore conditions. In the turbid nearshore areas where SPM concentration often exceeds 100 mg/l the OM fraction in association with the mineral particles is dominant, masking the smaller signal of fresh OM produced by primary production. In contrast, in the offshore stations the fresh OM components prevail and therefore explain most of the variability seen in the SPM concentration. POC and PON measurements represent bulk properties of the OM in suspension, combining compounds of various types from labile, semi-labile, to refractory OM as well as specific components such as TEPs and pigments. Our data demonstrate that biophysical flocculation cannot be explained by these bulk observables. However, a model-based separation between a more reactive labile and a less reactive mineral-associated fraction of POC, PON and specifically TEP is a productive approach to make the impact of OM on the flocculation process detectable under long-time field observations. From our data-model synthesis we learned that the median floc size increases only when fresh TEP becomes a substantial fraction of the SPM. With our study, we could resolve the contradiction that similar TEP concentrations result in different floc sizes in winter and summer. Our results document that fresh TEP is one of the important controls of particles settling in coastal waters.

POM is associated with the mineral fraction and primarily with phyllosilicates (clays). It is therefore no surprise that the POM concentration increases with SPM concentration in coastal waters where due to water depths below 20 m and changing turbulence levels from tidal currents and waves, significant exchanges between pelagic and sea bed material exist. The fresh POM, and more specifically the presence of fresh TEP in spring and summer is not associated with these minerals but rather with the phytoplankton activity. This fresh TEP is responsible for the formation of larger biophysical flocs in spring and summer in the high turbid areas rather than the total TEP concentration. The nearly absence of fresh TEP in winter as a glue after particle collisions limits the floc sizes. Our results underline that the different components of the SPM, which are mineral, OM, and living particles, form an integrated dynamic system with direct interactions and feedback controls.

Collecting data, such as SPM, POC, PON, and TEP concentrations, from samples in the oceans or coastal seas, is expensive and often biased toward good and moderate weather conditions. Especially, anomalous, short-term events can often not be captured as shipping schedules are planned long in advance. SPM concentration, however, as a key proxy, can be measured either by remote sensing or automated in-situ systems using optical or acoustical sensors.

Our approach could change the scope of in situ observations from merely the collection of data toward the improvement and validation of models that describe fundamental aspects of SPM composition in coastal seas. The availability of proxies could have important implications for future monitoring programs, as they may fill the lack of continuous long-term data of POM properties and as such could help to improve the efficiency of our monitoring systems by identifying more efficient locations for water sampling or for the deployment of observational instruments.

## Appendix A: Tables With Mean Values

The tables [A1–A3](#) contain the yearly and the winter (December till February), spring (March till May), summer (June till August) and autumn (September till November) averaged particulate and dissolved in situ measured data.

**Table A1**

*MOW1 (2004–2020), Geometric Mean and Multiplicative Standard Deviation for the Particulate and Dissolved Parameters (TDN: Total Dissolved Nitrogen, TDP: Total Dissolved Phosphate, Si: Silicate) and Arithmetic Mean and Standard Deviation for the Seabed Parameters*

	Year		Winter		Spring		Summer		Autumn	
	Mean	Std	Mean	Std	Mean	Std	Mean	Std	Mean	Std
Particulate parameters										
Hach Turbidity (FNU)	57	2.39	80	2.28	59	2.20	30	2.42	60	2.17
SPM-mass conc. (mg/l)	70	2.32	91	2.25	77	2.41	41	2.14	69	2.09
SPM-vol conc. (µl/l)	249	3.32	353	2.45	227	3.25	90	2.33	395	3.48
Median floc size (µm)	64	1.89	53	1.73	61	2.00	78	1.82	69	1.89
Effective floc density (mg/l)	246	2.48	370	2.11	228	2.46	117	2.02	320	2.30
POC conc. (mg/l)	2.62	2.05	2.91	2.10	3.20	2.01	1.61	1.66	2.56	1.97
PON conc. (mg/l)	0.35	1.99	0.38	2.04	0.44	1.93	0.23	1.61	0.33	1.97
TEP conc. (mg XG eq./l)	3.57	2.05	2.80	2.34	4.12	1.95	3.30	1.66	4.61	1.85
Chl-a conc. (µg/l)	5.75	2.50	3.47	1.94	12.94	1.93	8.81	1.66	3.78	2.46
Pheo-a conc. (µg/l)	0.41	2.36	0.41	2.58	0.58	1.96	0.28	1.86	0.34	2.47
POC:SPM (%)	3.81	1.39	3.25	1.28	4.07	1.44	4.60	1.40	3.72	1.31
PON:SPM (%)	0.50	1.46	0.40	1.28	0.55	1.49	0.66	1.49	0.45	1.31
TEP:SPM (g XG eq./g)	0.054	2.27	0.033	2.26	0.066	2.26	0.067	2.27	0.071	1.62
Dissolved parameters										
Salinity	31.6	1.03	31.7	1.03	30.6	1.02	31.8	1.02	32.5	1.02
DOC conc. (mg/l)	1.42	1.32	1.45	1.46	1.54	1.25	1.50	1.20	1.28	1.22
TDN conc. (µmol/l)	29.3	1.54	45.2	1.29	31.9	1.51	19.3	1.25	23.8	1.26
TDP conc. (µmol/l)	0.78	1.42	1.00	1.27	0.58	1.42	0.74	1.15	0.78	1.41
Si conc. (µmol/l)	11.08	1.82	18.5	1.29	9.81	1.54	4.54	1.54	14.0	1.26
Seabed parameters										
POC in sediment (%)	1.98	0.18	–	–	–	–	–	–	–	–
PON in sediment (%)	0.27	0.02	–	–	–	–	–	–	–	–

**Table A2**

*Idem Table A1 but Now for W05*

	Year		Winter		Spring		Summer		Autumn	
	Mean	Std	Mean	Std	Mean	Std	Mean	Std	Mean	Std
Particulate parameters										
Hach Turbidity (FNU)	3.88	2.87	9.34	1.79	1.56	3.15	2.36	1.81	4.42	2.51
SPM-mass conc. (mg/l)	8.5	1.82	13.6	1.67	7.7	1.64	5.6	1.55	9.3	1.75
SPM-vol conc. (µl/l)	41	1.82	61	1.98	40	1.77	24	1.08	35	1.47
Median floc size (µm)	136	1.51	101	1.40	146	1.20	284	1.03	134	1.43
Effective floc density (mg/l)	47	1.80	71	1.88	45	1.74	26	1.07	40	1.46
POC conc. (mg/l)	0.56	1.61	0.52	1.60	0.83	1.61	0.39	1.32	0.49	1.27
PON conc. (mg/l)	0.074	1.47	0.067	1.61	0.094	1.34	0.071	1.34	0.072	1.14
TEP conc. (mg XG eq./l)	0.94	1.84	0.83	2.14	1.65	1.55	1.02	1.41	0.75	1.61
Chl-a conc. (µg/l)	3.03	2.23	1.46	1.49	4.82	3.02	3.62	1.90	3.88	1.22
Pheo-a conc. (µg/l)	0.14	2.67	0.10	1.76	0.13	2.30	0.19	4.87	0.15	1.33
POC:SPM (%)	6.74	1.76	3.80	1.26	10.84	1.45	9.52	1.69	7.21	1.47

**Table A2**  
*Continued*

	Year		Winter		Spring		Summer		Autumn	
	Mean	Std	Mean	Std	Mean	Std	Mean	Std	Mean	Std
PON:SPM (%)	0.93	1.83	0.49	1.22	1.45	1.34	1.46	1.71	1.13	1.58
TEP:SPM (g XG eq./g)	0.124	2.08	0.077	2.07	0.253	1.49	0.153	1.52	0.111	2.01
Dissolved parameters										
Salinity	33.8	1.02	33.7	1.03	32.9	1.03	33.8	1.03	34.3	1.01
DOC conc.(mg/l)	1.10	1.34	1.08	1.53	1.52	1.20	1.07	1.23	1.01	1.18
TDN conc. (μmol/l)	14.7	1.72	25.5	1.44	18.2	1.18	9.5	1.62	12.4	1.54
TDP conc. (μmol/l)	0.48	1.47	0.69	1.26	0.47	1.17	0.37	1.29	0.44	1.52
Si conc. (μmol/l)	4.48	1.90	7.72	2.07	4.10	1.22	2.30	1.56	4.68	1.50
Seabed parameters										
POC in sediment (%)	1.80	0.28	–	–	–	–	–	–	–	–
PON in sediment (%)	0.26	0.03	–	–	–	–	–	–	–	–

**Table A3**  
*Idem Table A1 but Now for W08*

	Year		Winter		Spring		Summer		Autumn	
	Mean	Std	Mean	Std	Mean	Std	Mean	Std	Mean	Std
Particulate parameters										
Hach Turbidity (FNU)	1.74	1.93	2.44	1.94	0.98	1.64	1.16	1.94	2.03	1.46
SPM-mass conc. (mg/l)	3.72	1.46	4.74	1.36	3.48	1.30	2.74	1.47	3.96	1.28
SPM-vol conc. (μl/l)	23	1.84	39	1.57	15	1.32	11	1.13	21	1.55
Median floc size (μm)	148	1.44	119	1.21	175	1.08	187	1.04	162	1.70
Effective floc density (mg/l)	27	1.77	44	1.50	17	1.30	13	1.12	23	1.50
POC conc. (mg/l)	0.32	1.42	0.26	1.38	0.45	1.24	0.33	1.45	0.37	1.21
PON conc. (mg/l)	0.045	1.43	0.038	1.47	0.057	1.28	0.045	1.30	0.053	1.26
TEP conc. (mg XG eq./l)	0.62	1.66	0.32	1.54	0.79	1.21	0.58	1.59	0.81	1.46
Chl-a conc. (μg/l)	1.00	1.53	1.09	1.49	0.63	1.37	0.80	1.48	1.33	1.26
Pheo-a conc. (μg/l)	0.044	1.50	0.044	1.44	–	–	0.029	1.54	0.056	1.27
POC:SPM (%)	8.71	1.70	5.56	1.43	13.05	1.20	13.63	1.58	9.34	1.37
POC:SPM (%)	1.20	1.77	0.77	1.54	1.65	1.30	2.17	1.53	1.42	1.39
TEP:SPM (g XG eq./g)	0.169	1.85	0.075	1.52	0.226	1.29	0.173	1.82	0.21	1.64
Dissolved parameters										
Salinity	34.94	1.004	34.98	1.004	34.76	1.002	34.91	1.006	34.96	1.002
DOC conc.(mg/l)	0.96	1.35	1.09	1.53	1.02	1.09	0.98	1.26	0.82	1.13
TDN conc. (μmol/l)	8.3	1.67	15.3	1.28	6.13	1.18	5.4	1.54	7.3	1.25
TDP conc. (μmol/l)	0.33	1.59	0.59	1.31	0.24	1.15	0.23	1.15	0.27	1.38
Si conc. (μmol/l)	2.53	1.58	3.60	1.37	1.99	1.12	1.89	1.60	2.44	1.51
Seabed parameters										
POC in sediment (%)	1.09	0.38	–	–	–	–	–	–	–	–
PON in sediment (%)	0.19	0.08	–	–	–	–	–	–	–	–



### Appendix B: FSD by Mass

The FSD by mass in Figure B1 has been calculated following the method presented by Fall et al. (2021) and assuming a primary particle size of 2  $\mu\text{m}$  and a fractal dimension of 2. The figure shows that a significant part of the mass of the particles occurs in the smaller size classes and that the large particles have a low density.

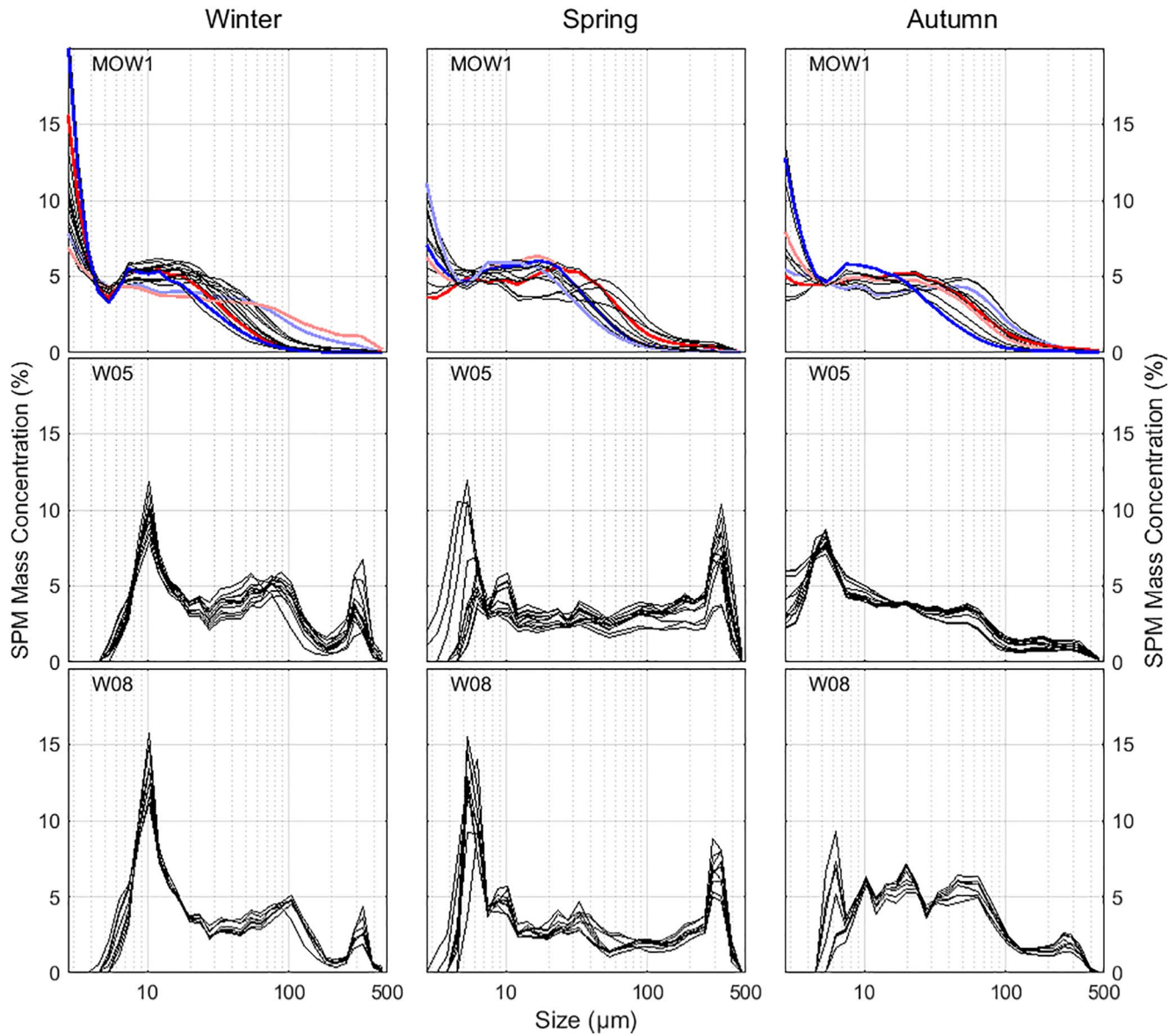


**Figure B1.** Similar as Figure 3 but now for the hourly particle size distribution by mass at about 2 m above the seabed during a tidal cycle at stations MOW1 (January, May, and September), W05 (December, May, and September), and W08 (December, May, and September). The mass concentration is normalized by dividing all values with the total mass. FSD at MOW1 are highlighted around maximum flood currents (light blue), HW slack (light red), maximum ebb currents (blue), and LW slack (red).

### Appendix C: Carbon Content of the TEP

Engel and Passow (2001) have reported that the carbon concentration of the transparent exopolymer particle (TEP;  $\text{mg/l}$ ) is linearly correlated with the TEP concentration (in  $\text{mg XG eq./l}$ ). The conversion factor between both depends on the chemical composition of the TEP and ranges from about 0.51 to 0.88 ( $\text{mg}/(\text{mg XG eq.})$ ). The slope of this regression line can be estimated by the particulate organic carbon (POC):TEP ratio. The ratio

derived from the measured POC and TEP concentrations is about 1 for all data, lower values are found in summer (0.64) and autumn (0.80) and higher ones in spring (2.08) and winter (1.28). Clearly, only the summer and autumn values are realistic and within the range reported by Engel and Passow (2001). The ratios derived from the POM:suspended particulate matter (SPM) model have a lower variability than those from the measurements. The fresh POC over fresh TEP ratio is approaching a constant value at SPM concentration above about 50 mg/l, whereas the ratio POC:TEP for the mineral-associated fraction (also derived from the POM:SPM model) is constant. The ratio for the fresh POC and fresh TEP is on average about 0.50 (spring), 0.38 (summer), 0.87 (autumn), and 0.45 (winter), corresponding with an overall slope factor of  $0.55 \pm 0.22$ . Similarly, the mineral-associated POC over TEP ratio for spring is 0.52, for summer 0.63, for autumn 0.54, and for winter 1.04 (on average  $0.68 \pm 0.24$ ). If all the POC is TEP, then these ratios provide an upper limit of the C content of fresh TEP. It is remarkable that the differences between fresh and mineral-associated ratios are small and that, notwithstanding the large uncertainties associated with the ratios (see Figures 5–8), the values of the slope factor derived from the model agree with the estimates from Engel and Passow (2001). The overall conversion of TEP concentration into carbon TEP concentration based on the model estimates is: C-TEP (mg/l) =  $0.57 \pm 0.21$  TEP (mg XG eq./l).

#### Appendix D: Monthly Model Parameters for TEP:SPM model

The table D1–A3 contain the monthly model  $K_{POM}$ ,  $f_1$  and  $f_2$  parameters for the TEP:SPM model. For the monthly fits 3 months are combined, centered around the month of interest.

<b>Table D1</b> Monthly Model Parameters for TEP			
$m_{POM} = 0.13$	$K_{POM}$ CI 95% [lower, upper]	$f_1$ CI 95% [lower, upper]	$f_2$ CI 95% [lower, upper]
January	4.25 [2.68, 6.00]	0.098 [0.059, 0.153]	0.251 [0.186, 0.319]
February	2.37 [1.66, 3.61]	0.078 [0.006, 0.198]	0.656 [0.465, 0.845]
March	1.91 [1.82, 1.99]	0.971 [0.583, 1.200]	0.444 [0.173, 0.793]
April	3.67 [2.12, 4.83]	0.489 [0.386, 0.641]	0.457 [0.265, 0.677]
May	4.96 [2.24, 7.11]	0.476 [0.386, 0.722]	0.090 [0.022, 0.154]
June	4.69 [2.58, 6.54]	0.412 [0.305, 0.576]	0.136 [0.065, 0.235]
July	4.78 [3.11, 6.80]	0.312 [0.233, 0.426]	0.297 [0.150, 0.531]
August	2.68 [1.03, 4.32]	0.371 [0.226, 0.714]	0.540 [0.392, 0.695]
September	1.91 [1.73, 2.10]	0.387 [0.285, 0.400]	0.526 [0.414, 0.653]
October	1.77 [1.56, 1.95]	0.291 [0.183, 0.435]	0.499 [0.406, 0.518]
November	1.99 [1.90, 2.13]	0.138 [0.058, 0.235]	0.346 [0.263, 0.441]
December	2.50 [1.46, 3.67]	0.081 [0.027, 0.147]	0.314 [0.251, 0.383]

Note. The units for  $K_{POM}$  are mg XG eq./l and for  $f_1$  and  $f_2$  [g XG eq./g POM].

### Appendix E: C:N Ratio

Figure E1 shows the seasonal C:N ratio calculated from the in situ measurements of POC and PON concentration and from the  $f_1$  and  $f_2$  model parameters for  $POC_i$  and  $POC_m$ .

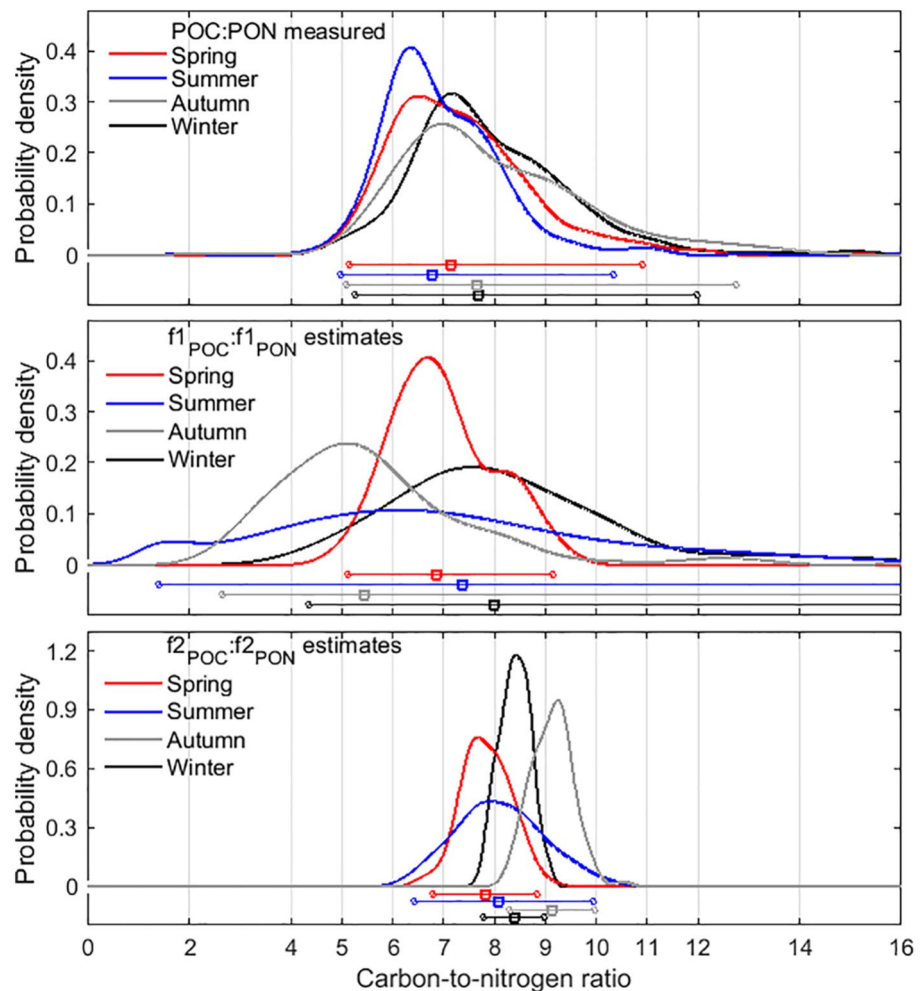


**Figure E1.** Probability density distribution of the POC:PON ratio from in situ measurements and of the Carbon to Nitrogen ratios of the model parameters  $f_1(POC):f_1(PON)$  and  $f_2(POC):f_2(PON)$ . The horizontal bars are the 95% CI.

#### Acknowledgments

This research was supported by the Belgian Science Policy (BELSPO) within the BRAIN-be program (BG-PART project), the Maritime Access Division of the Flemish Ministry of Mobility and Public Works (MOMO project), and the RBINS BGCMonit program. Scientific input from M. Schartau and R. Riethmüller are integrated in the research programs “Marine and polar life” and “Coastal zones at a time of global change” funded by the Helmholtz Association of German Research Centers. Ship time with the RV Belgica was provided by the BELSPO and the RBINS–OD Nature. The authors thank L. Naudts and his team (RBINS–MSO) for all technical aspects of instrumentation and moorings. The authors also would like to thank Carl Friedrichs and an anonymous reviewer for their constructive and encouraging comments.

#### Data Availability Statement

The long-term sensor data (SPM concentration and LISST) can be accessed through <https://doi.org/10.24417/bmcd.be:dataset:1250>. The tidal cycle data from water samples and LISST measurements used in this study can be found at <https://doi.pangaea.de/10.1594/PANGAEA.938674>. Sentinel-3 Ocean and Land Colour Instrument products are available through the Copernicus Online Data Access (CODA) service at <https://www.eumetsat.int/coda>.

#### References

- Adriaens, R., Zeelmaekers, E., Fettweis, M., Vanlierde, E., Vanlede, J., Stassen, P., et al. (2018). Quantitative clay mineralogy as provenance indicator for recent muds in the southern North Sea. *Marine Geology*, 398, 48–58. <https://doi.org/10.1016/j.margeo.2017.12.011>
- Agrawal, Y., & Pottsmith, H. (2000). Instruments for particle size and settling velocity observations in sediment transport. *Marine Geology*, 168, 89–114. [https://doi.org/10.1016/S0025-3227\(00\)00044-X](https://doi.org/10.1016/S0025-3227(00)00044-X)
- Allredge, A. L., Passow, U., & Logan, B. E. (1993). The abundance and significance of a class of large, transparent organic particles in the ocean. *Deep-Sea Research I*, 40, 1131–1140. [https://doi.org/10.1016/0967-0637\(93\)90129-Q](https://doi.org/10.1016/0967-0637(93)90129-Q)

- Andrews, S., Nover, D., & Schladow, S. (2010). Using laser diffraction data to obtain accurate particle size distributions: The role of particle composition. *Limnology and Oceanography: Methods*, *8*, 507–526. <https://doi.org/10.4319/lom.2010.8.507>
- Arndt, S., Jørgensen, B. B., LaRowe, D. E., Middelburg, J. J., Pancost, R. D., & Regnier, P. (2013). Quantifying the degradation of organic matter in marine sediments: A review and synthesis. *Earth-Science Reviews*, *123*, 53–86. <https://doi.org/10.1016/j.earscirev.2013.02.008>
- Bach, L. T., Stange, P., Taucher, J., Achterberg, E. P., Algueró-Muñiz, M., Horn, H., et al. (2019). The influence of plankton community structure on sinking velocity and remineralization rate of marine aggregates. *Global Biogeochemical Cycles*, *33*, 971–994. <https://doi.org/10.1029/2019GB006256>
- Baeteman, C., Scott, D. B., & Van Strydonck, M. (2002). Changes in coastal zone processes at a high sea-level stand: A late-Holocene example from Belgium. *Journal of Quaternary Science*, *17*, 547–559. <https://doi.org/10.1002/jqs.707>
- Baeye, M., & Fettweis, M. (2015). In situ observations of suspended particulate matter plumes at an offshore wind farm. *Geo-Marine Letters*, *35*, 247–255. <https://doi.org/10.1007/s00367-015-0404-8>
- Beardsley, R. C., Limeburner, R., & Rosenfeld, L. K. (1985). Introduction to CODE-2 moored array and large-scale data report (Technical Report WHOI-85-35, CODE Technical Report No 38, p. 234). Woods Hole Oceanographic Institution.
- Bhaskar, P. V., & Bhosle, N. B. (2006). Dynamics of transparent exopolymeric particles (TEP) and particle-associated carbohydrates in the Dona Paula bay, west coast of India. *Journal of Earth System Science*, *115*, 403–413. <https://doi.org/10.1007/BF02702869>
- Blattmann, T. M., Liu, Z., Zhang, Y., Zhao, Y., Haghypour, N., Montluçon, D. B., et al. (2019). Mineralogical control on the fate of continentally derived organic matter in the ocean. *Science*, *366*, 742–745. <https://doi.org/10.1126/science.aax5345>
- Bouillon, S., Yambélé, A., Spencer, R. G. M., Gillikin, D. P., Hernes, P. J., Six, J., et al. (2012). Organic matter sources, fluxes and greenhouse gas exchange in the Oubangui River (Congo River basin). *Biogeosciences*, *9*, 2045–2062. <https://doi.org/10.5194/bg-9-2045-2012>
- Braithwaite, K. M., Bowers, D. G., Nimmo-Smith, W. A. M., & Graham, G. W. (2012). Controls on floc growth in an energetic tidal channel. *Journal of Geophysical Research*, *117*, C02024. <https://doi.org/10.1029/2011JC007094>
- Buonassissi, C. J., & Dierssen, H. M. (2010). A regional comparison of particle size distributions and the power law approximation in oceanic and estuarine surface waters. *Journal of Geophysical Research*, *115*, C10028. <https://doi.org/10.1029/2010JC006256>
- Capuzzo, E., Lynam, C. P., Barry, J., Stephens, D., Forster, R. M., Greenwood, N., et al. (2018). A decline in primary production in the North Sea over 25 years, associated with reductions in zooplankton abundance and fish stock recruitment. *Global Change Biology*, *24*, e352–e364. <https://doi.org/10.1111/gcb.13916>
- Capuzzo, E., Stephens, D., Silva, T., Barry, J., & Forster, R. M. (2015). Decrease in water clarity of the southern and central North Sea during the 20th century. *Global Change Biology*, *21*, 2206–2214. <https://doi.org/10.1111/gcb.12854>
- Chen, Y., Wang, M., Zhou, X., Fu, H., Qu, X., & Zhu, D. (2021). Sorption fractionation of bacterial extracellular polymeric substances (EPS) on mineral surfaces and associated effects on phenanthrene sorption to EPS-mineral complexes. *Chemosphere*, *263*, 128264. <https://doi.org/10.1016/j.chemosphere.2020.128264>
- Chowdhury, C., Majumder, N., & Jana, T. K. (2016). Seasonal distribution and correlates of transparent exopolymer particles (TEP) in the waters surrounding mangroves in the Sundarbans. *Journal of Sea Research*, *112*, 65–74. <https://doi.org/10.1016/j.seares.2016.01.004>
- Cross, J., Nimmo-Smith, W. A. M., Torres, R., & Hosegood, P. J. (2013). Biological controls on resuspension and the relationship between particle size and the Kolmogorov length scale in a shallow coastal sea. *Marine Geology*, *343*, 29–38. <https://doi.org/10.1016/j.margeo.2013.06.014>
- Davies, E. J., Nimmo-Smith, W. A. M., Agrawal, Y. C., & Souza, A. J. (2012). LISST-100 response to large particles. *Marine Geology*, *307–310*, 117–122. <https://doi.org/10.1016/j.margeo.2012.03.006>
- Decho, A. W., & Gutierrez, T. (2017). Microbial extracellular polymeric substances (EPSs) in ocean systems. *Frontiers in Microbiology*, *8*(922). <https://doi.org/10.3389/fmicb.2017.00922>
- Deng, Z., He, Q., Safar, Z., & Chassagne, C. (2019). The role of algae in fine sediment flocculation: In-situ and laboratory measurements. *Marine Geology*, *413*, 71–84. <https://doi.org/10.1016/j.margeo.2019.02.003>
- Desmit, X., Nohe, A., Borges, A. V., Prins, T., De Cauwer, K., Lagring, R., et al. (2020). Changes in chlorophyll concentration and phenology in the North Sea in relation to de-eutrophication and sea surface warming. *Limnology & Oceanography*, *65*, 828–847. <https://doi.org/10.1002/lno.11351>
- Desmit, X., Thieu, V., Billen, G., Campuzano, F., Dulière, V., Garnier, J., et al. (2018). Reducing marine eutrophication may require a paradigmatic change. *The Science of the Total Environment*, *635*, 444–1466. <https://doi.org/10.1016/j.scitotenv.2018.04.181>
- Doerffer, R., & Schiller, H. (2007). The MERIS Case 2 water algorithm. *International Journal of Remote Sensing*, *28*, 517–535. <https://doi.org/10.1080/01431160600821127>
- Downing, J. (2006). Twenty-five years with OBS sensors: The good, the bad, and the ugly. *Continental Shelf Research*, *26*, 2299–2318. <https://doi.org/10.1016/j.csr.2006.07.018>
- Dyer, K. R. (1989). Sediment processes in estuaries: Future research requirements. *Journal of Geophysical Research: Oceans*, *94*, 14327–14339. <https://doi.org/10.1029/JC094iC10p14327>
- Ehrhardt, M., & Koeve, W. (1999). Determination of particulate organic carbon and nitrogen. In K. Grasshoff, K. Kremling, & M. Ehrhardt (Eds.), *Methods of seawater analysis* (3rd ed., pp. 437–444). Wiley. <https://doi.org/10.1002/9783527613984.ch17>
- Eisma, D., & Kalf, J. (1979). Distribution and particle size of suspended matter in the Southern Bight of the North Sea and the eastern channel. *Netherlands Journal of Sea Research*, *13*, 298–324. [https://doi.org/10.1016/0077-7579\(79\)90008-5](https://doi.org/10.1016/0077-7579(79)90008-5)
- Engel, A., Endres, S., Galgani, L., & Schartau, M. (2020). Marvelous marine microgels: On the distribution and impact of gel-like particles in the oceanic water-column. *Frontiers in Marine Science*, *7*, 405. <https://doi.org/10.3389/fmars.2020.00405>
- Engel, A., & Passow, U. (2001). Carbon and nitrogen content of transparent exopolymer particles (TEP) in relation to their Alcian Blue adsorption. *Marine Ecology Progress Series*, *219*, 1–10. <https://doi.org/10.3354/meps219001>
- Engel, A., & Schartau, M. (1999). Influence of transparent exopolymer particles (TEP) on sinking velocity of *Nitzschia closterium* aggregates. *Marine Ecology Progress Series*, *182*, 69–76. <https://doi.org/10.3354/meps182069>
- Engel, A., Thoms, S., Riebesell, U., Rochelle-Newall, E., & Zondervan, S. (2004). Polysaccharide aggregation as a potential sink of marine dissolved organic carbon. *Nature*, *428*, 929–932. <https://doi.org/10.1038/nature02453>
- Etcheber, H., Taillez, A., Abril, G., Garnier, J., Servais, P., Moatar, F., & Commarieu, M.-V. (2007). Particulate organic carbon in the estuarine turbidity maxima of the Gironde, Loire and seine estuaries: Origin and lability. *Hydrobiologia*, *588*, 245–259. <https://doi.org/10.1007/s10750-007-0667-9>
- EUMETSAT. (2019). Sentinel-3 product notice – OLCI level-2 ocean colour (EUM/OPS-SEN3/TEN/19/1068317). [https://www-cdn.eumetsat.int/files/2020-04/pdf\\_s3\\_pn\\_olci\\_l2m\\_001.pdf](https://www-cdn.eumetsat.int/files/2020-04/pdf_s3_pn_olci_l2m_001.pdf)
- Fall, K. A., Friedrichs, C. T., Massey, G. M., Bowers, D. G., & Smith, J. S. (2021). The importance of organic content to fractal floc properties in estuarine surface waters: Insights from video, LISST, and pump sampling. *Journal of Geophysical Research: Oceans*, *126*, e2020JC016787. <https://doi.org/10.1029/2020JC016787>



- Fettweis, M. (2008). Uncertainty of excess density and settling velocity of mud floes derived from in situ measurements. *Estuarine, Coastal and Shelf Science*, 78, 428–436. <https://doi.org/10.1016/j.ecss.2008.01.007>
- Fettweis, M., & Baeye, M. (2015). Seasonal variation in concentration, size and settling velocity of muddy marine floes in the benthic boundary layer. *Journal of Geophysical Research: Oceans*, 120, 5648–5667. <https://doi.org/10.1002/2014JC010644>
- Fettweis, M., Baeye, M., Van der Zande, D., Van den Eynde, D., & Lee, B. J. (2014). Seasonality of floe strength in the southern North Sea. *Journal of Geophysical Research: Oceans*, 119, 1911–1926. <https://doi.org/10.1002/2013JC009750>
- Fettweis, M., Francken, F., Pison, V., & Van den Eynde, D. (2006). Suspended particulate matter dynamics and aggregate sizes in a high turbidity area. *Marine Geology*, 235, 63–74. <https://doi.org/10.1016/j.margeo.2006.10.005>
- Fettweis, M., & Lee, B. J. (2017). Spatial and seasonal variation of biomineral suspended particulate matter properties in high-turbid nearshore and low-turbid offshore zones. *Water*, 9, 694. <https://doi.org/10.3390/w9090694>
- Fettweis, M., Monbaliu, J., Nechad, B., Baeye, M., & Van den Eynde, D. (2012). Weather and climate related spatial variability of high turbidity areas in the North Sea and the English Channel. *Methods in Oceanography*, 3–4, 25–39. <https://doi.org/10.1016/j.mio.2012.11.001>
- Fettweis, M., Riethmüller, R., Verney, R., Becker, M., Backers, J., Baeye, M., et al. (2019). Uncertainties associated with in situ long-term observations of suspended particulate matter concentration using optical and acoustic sensors. *Progress in Oceanography*, 178, 102162. <https://doi.org/10.1016/j.pocean.2019.102162>
- Fettweis, M., & Van den Eynde, D. (2003). The mud deposits and the high turbidity in the Belgian–Dutch coastal zone, Southern Bight of the North Sea. *Continental Shelf Research*, 23, 669–691. [https://doi.org/10.1016/S0278-4343\(03\)00027-X](https://doi.org/10.1016/S0278-4343(03)00027-X)
- Frigstad, H., Andersen, T., Hessen, D. O., Naustvoll, L.-J., Johnsen, T. M., & Bellerby, R. G. J. (2011). Seasonal variation in marine C:N:P stoichiometry: Can the composition of seston explain stable Redfield ratios? *Biogeosciences*, 8, 2917–2933. <https://doi.org/10.5194/bg-8-2917-2011>
- Fuchs, E., Zimmerman, R. C., & Jaffe, J. S. (2002). The effect of elevated levels of phaeophytin in natural water on variable fluorescence measured from phytoplankton. *Journal of Plankton Research*, 24, 1221–1229. <https://doi.org/10.1093/plankt/24.11.1221>
- Fugate, D. C., & Friedrichs, C. T. (2002). Determining concentration and fall velocity of estuarine particle populations using ADV, OBS and LISST. *Continental Shelf Research*, 22, 1867–1886. [https://doi.org/10.1016/S0278-4343\(02\)00043-2](https://doi.org/10.1016/S0278-4343(02)00043-2)
- Fukao, T., Kimoto, K., & Kotani, Y. (2010). Production of transparent exopolymer particles by four diatom species. *Fisheries Science*, 76, 755–760. <https://doi.org/10.1007/s12562-010-0265-z>
- Gartner, J. W., Cheng, R. T., Wang, P. F., & Richter, K. (2001). Laboratory and field evaluations of the LISST-100 instrument for suspended particle size distributions. *Marine Geology*, 175, 199e219. [https://doi.org/10.1016/S0025-3227\(01\)00137-2](https://doi.org/10.1016/S0025-3227(01)00137-2)
- Graham, G. W., Davies, E. J., Nimmo-Smith, W. A. M., Bowers, D. G., & Braithwaite, K. M. (2012). Interpreting LISST-100X measurements of particles with complex shape using digital in-line holography. *Journal of Geophysical Research: Oceans*, 117, C05034. <https://doi.org/10.1029/2011JC007613>
- Hemingway, G. D., Rothman, D. H., Grant, K. E., Rosengard, S. Z., Eglinton, T. I., Derry, L. A., & Galy, V. V. (2019). Mineral protection regulates long-term global preservation of natural organic carbon. *Nature*, 570, 228–231. <https://doi.org/10.1038/s41586-019-1280-6>
- Hendriks, H. C. M., van Prooijen, B. C., Aarninkhof, S. G. J., & Winterwerp, J. C. (2020). How human activities affect the fine sediment distribution in the Dutch Coastal Zone seabed. *Geomorphology*, 367, 107314. <https://doi.org/10.1016/j.geomorph.2020.107314>
- Horemans, D. M. L., Dijkstra, Y. M., Schuttelaars, H. M., Sabbe, K., Vyverman, W., Meire, P., & Cox, T. J. S. (2021). Seasonal variations in flocculation and erosion affecting the large-scale suspended sediment distribution in the Scheldt estuary: The importance of biotic effects. *Journal of Geophysical Research: Oceans*, 126, e2020JC016805. <https://doi.org/10.1029/2020JC016805>
- Howarth, M. J., Dyer, K. R., Joint, I. R., Hydes, D. J., Purdie, D. A., Edmunds, H., et al. (1994). Seasonal cycles and their spatial variability. *Philosophical Transactions of the Royal Society A*, 343, 383–403. <https://doi.org/10.1098/rsta.1993.0054>
- Høyer, J. L., & Karagali, I. (2016). Sea surface temperature climate data record for the North Sea and Baltic Sea. *Journal of Climate*, 29, 2529–2541. <https://doi.org/10.1175/JCLI-D-15-0663.1>
- Jachlewski, S., Jachlewski, W. D., Linne, U., Brasen, C., Wingender, J., & Siebers, B. (2015). Isolation of extracellular polymeric substances from biofilms of the thermoacidophilic archaeon *Sulfolobus acidocaldarius*. *Frontiers in Bioengineering and Biotechnology*, 3, 123. <https://doi.org/10.3389/fbioe.2015.00123>
- Jago, C. F., Bale, A. J., Green, M. O., Howarth, M. J., Jones, S. E., McCave, I. N., et al. (1993). Resuspension processes and seston dynamics, southern North Sea. In H. Charnock, K. R. Dyer, J. M. Huthnance, P. S. Liss, J. H. Simpson & P. B. Tett (Eds.), *Understanding the North Sea system*. Springer Verlag. [https://doi.org/10.1007/978-94-011-1236-9\\_8](https://doi.org/10.1007/978-94-011-1236-9_8)
- Jago, C. F., Kennaway, G. M., Novarino, G., & Jones, S. E. (2007). Size and settling velocity of suspended floes during a phaeocystis bloom in the tidally stirred Irish Sea, NW European Shelf. *Marine Ecology Progress Series*, 345, 51–62. <https://doi.org/10.3354/meps07006>
- Jaiser, R., Dethloff, K., Handorf, D., Rinke, H., & Cohen, J. (2012). Impact of sea ice cover changes on the Northern Hemisphere atmospheric winter circulation. *Tellus A: Dynamic Meteorology and Oceanography*, 64, 11595. <https://doi.org/10.3402/tellusa.v64i0.11595>
- Johnston, R. J., & Semple, R. K. (1983). Classification using information statistics. In *Concepts and techniques in modern geography* (Vol. 37, p. 43). GeoBooks.
- Kalbitz, K., Schwesig, D., Rethemeyer, J., & Matzner, E. (2005). Stabilization of dissolved organic matter by sorption to the mineral soil. *Soil Biology and Biochemistry*, 37, 1319–1331. <https://doi.org/10.1016/j.soilbio.2004.11.028>
- Keil, R. G., Montluçon, D. B., Prah, F. G., & Hedges, J. I. (1994). Sorptive preservation of labile organic matter in marine sediments. *Nature*, 370, 549–552. <https://doi.org/10.1038/370549a0>
- Keyvani, A., & Strom, K. (2014). Influence of cycles of high and low turbulent shear on the growth rate and equilibrium size of mud floes. *Marine Geology*, 354, 1–14. <https://doi.org/10.1016/j.margeo.2014.04.010>
- Lacroix, G., Ruddick, K., Ozer, J., & Lancelot, C. (2004). Modelling the impact of the Scheldt and Rhine/Meuse plumes on the salinity distribution in Belgian waters (southern North Sea). *Journal of Sea Research*, 52, 149–163. <https://doi.org/10.1016/j.seares.2004.01.003>
- Lai, H., Fang, H., Huang, L., He, G., & Reible, D. (2018). A review on sediment bioflocculation: Dynamics, influencing factors and modeling. *The Science of the Total Environment*, 642, 1184–1200. <https://doi.org/10.1016/j.scitotenv.2018.06.101>
- Lancelot, C., Spitz, Y., Gypens, N., Ruddick, K., Becquevort, S., Rousseau, V., et al. (2005). Modelling diatom and phaeocystis blooms and nutrient cycles in the Southern Bight of the North Sea: The MIRO model. *Marine Ecology Progress Series*, 289, 63–78. <https://doi.org/10.3354/meps289063>
- Lavigne, H., Van der Zande, D., Ruddick, K., Dos Santos, J. C., Gohin, F., Brotas, V., & Kratzer, S. (2021). Quality-control tests for OC4, OC5 and NIR-red satellite chlorophyll-a algorithms applied to coastal waters. *Remote Sensing of Environment*, 255, 112237. <https://doi.org/10.1016/j.rse.2020.112237>
- Lee, B. J., Fettweis, M., Toorman, E., & Molz, F. J. (2012). Multimodality of a particle size distribution of cohesive suspended particulate matters in a coastal zone. *Journal of Geophysical Research: Oceans*, 117, C03014. <https://doi.org/10.1029/2011JC007552>

- Lee, B. J., Kim, J., Hur, J., Choi, I.-H., Toorman, E., Fettweis, M., & Choi, J. W. (2019). Seasonal dynamics of organic matter composition and its effects on suspended sediment flocculation in river water. *Water Resources Research*, 55, 6968–6985. <https://doi.org/10.1029/2018WR024486>
- Lee, J. H., Lee, W. C., Kim, H. C., Jo, N., Jang, H. K., Kang, J. J., et al. (2020). Transparent exopolymer particle (TEPs) dynamics and contribution to particulate organic carbon. *Water*, 12, 1057. <https://doi.org/10.3390/w12041057>
- Liénard, C., Savoye, N., Bozec, Y., Breton, E., Conan, P., David, V., et al. (2017). Dynamics of particulate organic matter composition in coastal systems: A spatio-temporal study at multi-systems scale. *Progress in Oceanography*, 156, 221–239. <https://doi.org/10.1016/j.pocean.2017.03.001>
- Liley, J. B. (1992). Fitting size distributions to optical particle counter data. *Aerosol Science and Technology*, 17, 84–92. <https://doi.org/10.1080/02786829208959562>
- Logan, B. E., Passow, U., Alldredge, A. L., Grossart, S. M., & Simont, M. (1995). Rapid formation and sedimentation of large aggregates is predictable from coagulation rates (half-lives) of transparent exopolymer particles (TEP). *Deep-Sea Research II*, 42, 203–214. [https://doi.org/10.1016/0967-0645\(95\)00012-F](https://doi.org/10.1016/0967-0645(95)00012-F)
- Long, R. A., & Azam, F. (1996). Abundant protein-containing particles in the sea. *Aquatic Microbial Ecology*, 10, 213–221. <https://doi.org/10.3354/ame010213>
- Maerz, J., Hofmeister, R., van der Lee, E. M., Gräwe, U., Riethmüller, R., & Wirtz, K. W. (2016). Maximum sinking velocities of suspended particulate matter in a coastal transition zone. *Biogeosciences*, 13, 4863–4876. <https://doi.org/10.5194/bg-13-4863-2016>
- Maggi, F., & Tang, F. H. M. (2015). Analysis of the effect of organic matter content on the architecture and sinking of sediment aggregates. *Marine Geology*, 363, 102–111. <https://doi.org/10.1016/j.margeo.2015.01.017>
- Malarkey, J., Baas, J. H., Hope, J. A., Aspden, R. J., Parsons, D. R., Peakall, J., et al. (2015). The pervasive role of biological cohesion in bedform development. *Nature Communications*, 6, 6257. <https://doi.org/10.1038/ncomms7257>
- Malpezzi, M. A., Sanford, L. P., & Crump, B. C. (2013). Abundance and distribution of transparent exopolymer particles in the estuarine turbidity maximum of Chesapeake Bay. *Marine Ecology Progress Series*, 486, 23–35. <https://doi.org/10.3354/meps10362>
- Manning, A. J., & Bass, S. J. (2006). Variability in cohesive sediment settling fluxes: Observations under different estuarine tidal conditions. *Marine Geology*, 235, 177–192. <https://doi.org/10.1016/j.margeo.2006.10.013>
- Manning, A. J., Baugh, J. V., Spearman, J. R., & Whitehouse, R. J. S. (2010). Flocculation settling characteristics of mud: Sand mixtures. *Ocean Dynamics*, 60, 237–253. <https://doi.org/10.1007/s10236-009-0251-0>
- Manning, A. J., Van Kessel, T., Melotte, J., Sas, M., Winterwerp, H., & Pidduck, E. L. (2011). On the consequence of a new tidal dock on the sedimentation regime in the Antwerpen area of the Lower Sea Scheldt. *Continental Shelf Research*, 31, S150–S164. <https://doi.org/10.1016/j.csr.2010.10.008>
- Mari, X., & Burd, A. (1998). Seasonal size spectra of transparent exopolymeric particles (TEP) in a coastal sea and comparison with those predicted using coagulation theory. *Marine Ecology Progress Series*, 163, 63–76. <https://doi.org/10.3354/meps171063>
- Mari, X., Passow, U., Migon, C., Burd, A. B., & Legendre, L. (2017). Transparent exopolymer particles: Effects on carbon cycling in the ocean. *Progress in Oceanography*, 151, 13–37. <https://doi.org/10.1016/j.pocean.2016.11.002>
- Mari, X., & Robert, M. (2008). Metal induced variations of TEP sticking properties in the southwestern lagoon of New Caledonia. *Marine Chemistry*, 110, 98–108. <https://doi.org/10.1016/j.marchem.2008.02.012>
- Mari, X., Rochelle-Newall, E., Torrétou, J.-P., Pringault, O., Jouon, A., & Migon, C. (2007). Water residence time: A regulatory factor of the DOM to POM transfer efficiency. *Limnology & Oceanography*, 52, 808–819. <https://doi.org/10.4319/lo.2007.52.2.0808>
- May, C. L., Koseff, J. R., Lucas, L. V., Cloern, J. E., & Schoellhamer, D. H. (2003). Effects of spatial and temporal variability of turbidity on phytoplankton blooms. *Marine Ecology Progress Series*, 254, 111–128. <https://doi.org/10.3354/meps254111>
- Mayer, L. M. (1994). Relationships between mineral surfaces and organic carbon concentrations in soils and sediments. *Chemical Geology*, 114, 347–363. [https://doi.org/10.1016/0009-2541\(94\)90063-9](https://doi.org/10.1016/0009-2541(94)90063-9)
- Mietta, F., Chassagne, C., Manning, A. J., & Winterwerp, J. C. (2009). Influence of shear rate, organic matter content, pH and salinity on mud flocculation. *Ocean Dynamics*, 59, 751–763. <https://doi.org/10.1007/s10236-009-0231-4>
- Mikkelsen, O., Hill, P., & Milligan, T. (2006). Single-grain, microfloc and macrofloc volume variations observed with a LISST-100 and a digital floc camera. *Journal of Sea Research*, 55, 87–102. <https://doi.org/10.1016/j.seares.2005.09.003>
- Mikkelsen, O. A., Curran, K. J., Hill, P. S., & Milligan, T. G. (2007). Entropy analysis of in situ particle size spectra. *Estuarine, Coastal and Shelf Science*, 72, 615–630. <https://doi.org/10.1016/j.ecss.2006.11.027>
- Milliman, J. D., Quichun, X., & Zuosheng, Y. (1984). Transfer of particulate organic carbon and nitrogen from Yangtze River to the ocean. *American Journal of Science*, 284, 824–834. <https://doi.org/10.2475/ajs.284.7.824>
- Morelle, J., Schapira, M., Françoise, S., Courtay, G., Orvain, F., & Clauquin, P. (2018). Dynamics of exopolymeric carbon pools in relation with phytoplankton succession along the salinity gradient of a temperate estuary (France). *Estuarine, Coastal and Shelf Science*, 209, 18–29. <https://doi.org/10.1016/j.ecss.2018.05.008>
- Neukermans, G., Ruddick, K., Loisel, H., & Roose, P. (2012). Optimization and quality control of suspended particulate matter concentration measurement using turbidity measurements. *Limnology and Oceanography: Methods*, 10, 1011–1023. <https://doi.org/10.4319/lom.2012.10.1011>
- Neumann, A., Hass, H. C., Möbius, J., & Naderipour, C. (2019). Ballasted flocs capture pelagic primary production and alter the local sediment characteristics in the coastal German Bight (North Sea). *Geosciences*, 9, 344. <https://doi.org/10.3390/geosciences9080344>
- Nohe, A., Goffin, A., Tyberghein, L., Lagring, R., De Cauwer, K., Vyverman, W., & Sabbe, K. (2020). Marked changes in diatom and dinoflagellate biomass, composition and seasonality in the Belgian part of the North Sea between the 1970s and 2000s. *The Science of the Total Environment*, 716, 136316. <https://doi.org/10.1016/j.scitotenv.2019.136316>
- Nosaka, Y., Yamashita, Y., & Suzuki, K. (2017). Dynamics and origin of transparent exopolymer particles in the Oyashio region of the western subarctic Pacific during the spring diatom bloom. *Frontiers in Marine Science*, 4, 79. <https://doi.org/10.3389/fmars.2017.00079>
- Ortega-Retuerta, E., Marrasé, C., Muñoz-Fernández, A., Sala, M. M., Simó, R., & Gasol, J. M. (2018). Seasonal dynamics of transparent exopolymer particles (TEP) and their drivers in the coastal NW Mediterranean Sea. *The Science of the Total Environment*, 631–632, 180–190. <https://doi.org/10.1016/j.scitotenv.2018.02.341>
- Pache, T., Brockamp, O., & Clauer, N. (2008). Varied pathways of river-borne clay minerals in a near-shore marine region: A case study of sediments from the Elbe- and Weser rivers, and the SE North Sea. *Estuarine, Coastal and Shelf Science*, 78, 563–575. <https://doi.org/10.1016/j.ecss.2008.01.016>
- Passow, U. (2000). Formation of transparent exopolymer particles, TEP, from dissolved precursor material. *Marine Ecology Progress Series*, 192, 1–11. <https://doi.org/10.3354/meps192001>
- Passow, U. (2002). Transparent exopolymer particles (TEP) in aquatic environments. *Progress in Oceanography*, 55, 287–333. [https://doi.org/10.1016/S0079-6611\(02\)00138-6](https://doi.org/10.1016/S0079-6611(02)00138-6)
- Passow, U., & Alldredge, A. L. (1995). A dye-binding assay for the spectrophotometric measurement of transparent exopolymer particles. *Limnology & Oceanography*, 40, 1326–1335. <https://doi.org/10.4319/lo.1995.40.7.1326>

- Ramaiah, N., Yoshikawa, T., & Furuya, K. (2001). Temporal variations in transparent exopolymer particles (TEP) associated with a diatom spring bloom in a subarctic ria in Japan. *Marine Ecology Progress Series*, 212, 79–88. <https://doi.org/10.3354/meps212079>
- Röttgers, R., Heymann, K., & Krasemann, H. (2014). Suspended matter concentrations in coastal waters: Methodological improvements to quantify individual measurement uncertainty. *Estuarine, Coastal and Shelf Science*, 151, 148–155. <https://doi.org/10.1016/j.ecss.2014.10.010>
- Rousseau, V., Leynaert, A., Daoud, N., & Lancelot, C. (2002). Diatom succession, silicification and silicic acid availability in Belgian coastal waters (southern North Sea). *Marine Ecology Progress Series*, 236, 61–73. <https://doi.org/10.3354/meps236061>
- Schartau, M., Engel, A., Schröter, J., Thoms, S., Völker, C., & Wolf-Gladrow, D. (2007). Modelling carbon overconsumption and the formation of extracellular particulate organic carbon. *Biogeosciences*, 4, 433–454. <https://doi.org/10.5194/bg-4-433-2007>
- Schartau, M., Riethmüller, R., Flöser, G., van Beusekom, J. E. E., Krasemann, H., Hofmeister, R., & Wirtz, K. (2019). On the separation between inorganic and organic fractions of suspended matter in a marine coastal environment. *Progress in Oceanography*, 171, 231–250. <https://doi.org/10.1016/j.pocean.2018.12.011>
- Schwarz, C., Cox, T. J. S., Van Engeland, T., Van Oevelen, D., Van Belzen, J., van de Koppel, J., et al. (2017). Field estimates of flocc dynamics and settling velocities in a tidal creek with significant along-channel gradients in velocity and SPM. *Estuarine, Coastal and Shelf Science*, 197, 221–235. <https://doi.org/10.1016/j.ecss.2017.08.041>
- Shen, X., Toorman, E. A., Lee, B. J., & Fettweis, M. (2018). Biophysical flocculation of suspended particulate matters in Belgian coastal zones. *Journal of Hydrology*, 567, 238–252. <https://doi.org/10.1016/j.jhydrol.2018.10.028>
- Shen, X., Toorman, E. A., Lee, B. J., & Fettweis, M. (2019). An approach to modeling biofilm growth during the flocculation of suspended cohesive sediments. *Journal of Geophysical Research: Ocean*, 124, 4098–4116. <https://doi.org/10.1029/2018JC014493>
- Skinnebach, K. H., Fruergaard, M., & Andersen, T. J. (2020). Biological effects on flocculation of fine-grained suspended sediment in natural seawater. *Estuarine, Coastal and Shelf Science*, 228, 106395. <https://doi.org/10.1016/j.ecss.2019.106395>
- Smith, D. C., Simon, M., Alldredge, A. L., & Azam, F. (1992). Intense hydrolytic enzyme activity on marine aggregates and implications for rapid particle dissolution. *Nature*, 359, 139–142. <https://doi.org/10.1038/359139a0>
- Smith, S. J., & Friedrichs, C. T. (2011). Size and settling velocities of cohesive flocs and suspended sediment aggregates in a trailing suction hopper dredge plume. *Continental Shelf Research*, 31, S50–S63. <https://doi.org/10.1016/j.csr.2010.04.002>
- Stavn, R. H., Rick, H. J., & Falster, A. V. (2009). Correcting the errors from variable sea salt retention and water of hydration in loss on ignition analysis: Implications for studies of estuarine and coastal waters. *Estuarine, Coastal and Shelf Science*, 81, 575–582. <https://doi.org/10.1016/j.ecss.2008.12.017>
- Tang, F. H. M., & Maggi, F. (2016). A mesocosm experiment of suspended particulate matter dynamics in nutrient- and biomass-affected waters. *Water Research*, 89, 76–86. <https://doi.org/10.1016/j.watres.2015.11.033>
- Tran, D., & Strom, K. (2017). Suspended clays and silts: Are they independent or dependent fractions when it comes to settling in a turbulent suspension? *Continental Shelf Research*, 138, 81–94. <https://doi.org/10.1016/j.csr.2017.02.011>
- van der Zee, C., & Chou, L. (2005). Seasonal cycling of phosphorus in the Southern Bight of the North Sea. *Biogeosciences*, 2, 27–42. <https://doi.org/10.5194/bg-2-27-2005>
- Van Engeland, T., Soetaert, K., Knuijt, A., Laane, R. W. P. M., & Middelburg, J. J. (2010). Dissolved organic nitrogen dynamics in the North sea: A time series analysis (1995–2005). *Estuarine, Coastal and Shelf Science*, 89, 31–42. <https://doi.org/10.1016/j.ecss.2010.05.009>
- van Maren, D. S., van Kessel, T., Cronin, K., & Sittoni, L. (2015). The impact of channel deepening and dredging on estuarine sediment concentration. *Continental Shelf Research*, 95, 1–14. <https://doi.org/10.1016/j.csr.2014.12.010>
- Verdugo, P. (2012). Marine microgels. *Annual Review of Marine Science*, 4, 375–400. <https://doi.org/10.1146/annurev-marine-120709-142759>
- Verney, R., Lafite, R., & Brun-Cottan, J. (2009). Flocculation potential of estuarine particles: The importance of environmental factors and of the spatial and seasonal variability of suspended particulate matter. *Estuaries and Coasts*, 32, 678–693. <https://doi.org/10.1007/s12237-009-9160-1>
- Winterwerp, J., Manning, A., Martens, C., de Mulder, T., & Vanlede, J. (2006). A heuristic formula for turbulence-induced flocculation of cohesive sediment. *Estuarine, Coastal and Shelf Science*, 68, 195–207. <https://doi.org/10.1016/j.ecss.2006.02.003>
- Winterwerp, J. C. (1998). A simple model for turbulence induced flocculation of cohesive sediment. *Journal of Hydraulic Research*, 36, 309–326. <https://doi.org/10.1080/00221689809498621>
- Zhang, Y., Ren, J., Zhang, W., & Wu, J. (2021). Importance of salinity-induced stratification on flocculation in tidal estuaries. *Journal of Hydrology*, 596, 126063. <https://doi.org/10.1016/j.jhydrol.2021.126063>
- Zhou, J., Mopper, K., & Passow, U. (1998). The role of surface-active carbohydrates in the formation of transparent exopolymer particles by bubble adsorption of seawater. *Limnology & Oceanography*, 43, 1860–1871. <https://doi.org/10.4319/lo.1998.43.8.1860>
- Zuther, M., Brockamp, O., & Clauer, N. (2000). Composition and origin of clay minerals in Holocene sediments from the south-eastern North Sea. *Sedimentology*, 47, 119–134. <https://doi.org/10.1046/j.1365-3091.2000.00282.x>